Methodologies for Characterizing Strain Fields Resulting from Focused Ultrasound Treatments in Mouse Achilles Tendon using Ultrasound Imaging and Digital Image Correlation

Steven A. Salazar

Thesis submitted to the Faculty of the
Virginia Polytechnic Institute and State University
in partial fulfillment of the requirements for the degree of

Master of Science
in
Engineering Mechanics

Vincent M. Wang, Chair
Eli Vlaisavljevich
Christopher B. Arena

July 7, 2022
Blacksburg, Virginia
Keywords: Digital Image Correlation, Focused Ultrasound, Tendinopathy

Methodologies for Characterizing Strain Fields Resulting from Focused Ultrasound Treatments in Mouse Achilles Tendon using Ultrasound Imaging and Digital Image Correlation

Steven A. Salazar

(ABSTRACT)

Tendinopathy is a common pathology of tendons characterized by pain and a decrease in function resulting from changes in the tissue's structure and/or composition due to injury. Diagnosis of tendinopathy is determined by the qualitative analysis of a trained physician usually with assistance from an imaging modality. Although physicians can often identify tendinopathy, there are no quantitative metrics to evaluate tendon fatigue, damage, or healing. Physical therapy (PT) is a common treatment for patients with tendinopathy, and recent studies have investigated Focused Ultrasound (FUS) for its treatment of tendons. Developments in the use of FUS as a therapeutic have led to studies of the underlying mechanisms by which it operates.

Digital Image Correlation (DIC) is a non-contact method of quantifying tissue displacements and strains of a deforming material using high resolution imaging DIC programs can evaluate and interpolate strain data by applying statistical image processing algorithms and solid continuum mechanics principles using a set of

sequential image frames capturing the mechanical deformation of the specimen during testing.

The studies presented in this thesis investigate methodologies for using DIC with ultrasound imaging of mouse Achilles tendons to characterize strains resulting from FUS therapies. The first method is based upon an orthogonal configuration of therapy and imaging transducers while the second investigates a coaxial experimental configuration. This work explores DIC as a viable means of quantifying the mechanical stimulation caused by FUS therapies on tendon tissue through ultrasound imaging to better understand the underlying mechanisms of FUS therapy.

Methodologies for Characterizing Strain Fields Resulting from Focused Ultrasound Treatments in Mouse Achilles Tendon using Ultrasound Imaging and Digital Image Correlation

Steven A. Salazar

(GENERAL AUDIENCE ABSTRACT)

Tendinopathy is a common injury that many people will experience in their lifetime. Pain and swelling are common symptoms and can make daily actions uncomfortable to perform. Physical therapy (PT) is one of the most common ways to help relieve the symptoms of this condition. A therapy being investigated to help treat tendinopathy utilizes Focused Ultrasound (FUS) technology to help the healing process. PT can be difficult and painful for those experiencing tendinopathy, but if a therapeutic like FUS could mimic the effects of PT, then some patients would not need to perform these physically demanding tasks. To understand if this treatment is viable, we need to better understand the underlying mechanisms by which it operates. Therefore, we are investigating the mechanical stimulation that FUS imparts on tendons because it is believed that the mechanical stimulations from exercise are a primary contributor to healing. Specifically, we want to evaluate the kind of strains applied by FUS therapies to inform decisions about dosage. One method uses Digital Image Correlation (DIC). DIC is a method of evaluating displacements and strains using non-contact high resolution imaging. DIC works using statistically motivated algorithms to calculate the deformation between subsequent video frames in a given material undergoing a state of stress. Using this technology along with ultrasound imaging, this work gives a

preliminary exploration of using DIC as a means of quantifying strain to better understand the underlying mechanisms of the mechanical stimulations caused by FUS therapy

Acknowledgements

I would first like to thank Dr. Vincent Wang for his support, guidance, and mentorship which has helped me to become a better scientist and engineer. I would also like to extend thanks to all my peers across labs who helped me through the project on tasks both small and large. Particularly I would like to thank Chitra Meduri who was both a mentor and friend to me. To my friends and family whose unending support helped propel me through my academic career and both the good and hard times that came and went - I am forever grateful.

Contents

Chapter 1

Introduction

Evidence of clinical efficacy in the use of Focused Ultrasound (FUS) as a therapeutic has led to studies of the underlying mechanisms by which it operates. FUS can be roughly categorized in some application spaces by whether it produces primarily mechanical or thermal energy and whether it produces a high or low pressure [9, 38]. The applications of varying these outputs from the transducer range from ablation therapies to neuromodulation as well as many other bioeffects that are under investigation [9, 16, 24].

This work presented herein concentrates on developing a methodology to improve our understanding of the underlying mechanisms of FUS in the context of using it as a therapy for tendinopathy. Specifically, this work investigates the use of Digital Image Correlation (DIC) with ultrasound (US) imaging to quantify and characterize the types of strain fields produced by FUS on tendon tissue in a mouse model. Other work which investigates the mechanical properties and deformations of larger structures, including tendons, in humans using US speckle tracking has been done for some standard mechanical testing procedures [12, 13]. Recent work has begun to validate this imaging methodology for smaller tendon structures in human knee models [12, 20]. However, few studies have investigated the mechanical and thermal effects of FUS, nor the application of DIC with US to evaluate those effects. Additionally, these methods have not yet been investigated at the scale of murine tendon tissue. This work uses an ex vivo mouse Achilles tendon model with the goal of developing a preliminary methodology to quantify

and characterize the strains that result from a novel FUS therapy through US imaging and DIC analysis.

1.1 Tendinopathy & FUS Therapy

Tendinopathy is a common pathology of tendons characterized by pain and a decrease in function due to changes in the tissue's composition and structure typically resulting from physically demanding activities that would engage the tendon [19]. The cause of tendinopathy has not been identified fully but a commonly accepted contributing factor is overuse [15, 19, 25]. As such, there is no universal standard system used by the medical community to identify tendinopathy. This is due to the several varying pathologies and symptoms the term encompasses in addition to the qualitative nature of its diagnosis. Instead, tendinopathy includes broad diagnoses determined by qualitative analysis of physicians. The diagnosis includes physical examinations, and is almost always supplemented by patient history, imaging, and other means to categorize a patient's specific pathology [16, 22].

Diagnosis of tendinopathy typically involves an imaging modality like magnetic resonance imaging (MRI) or grayscale ultrasonography (GR-US) [16, 35]. Imaging is one of the primary tools used by physicians to identify tendinopathy; however, imaging protocols cannot currently supplant the clinical diagnosis of a physician and it remains a diagnostic tool. Currently, both the diagnosis and treatment of

tendinopathy remains largely qualitative while attempts to develop quantitative measures of musculoskeletal fatigue are still being developed [25].

Physical therapy (PT) is a commonly suggested treatment, but its clinical significance is largely supported by qualitative evidence [2, 10]. Exercise is considerably effective compared to other treatments, and the underlying mechanisms that contribute to the healing effects of treatments in PT largely remain unknown [2, 10, 19]. PT is among few treatment options that have shown symptomatic relief long term, making the need for better understanding tendon healing a prominent long term aim of these preliminary investigations [28].

A novel treatment being investigated for tendinopathy is the application of FUS as a therapeutic. Currently there are limited resources available that have identified safe and effective dosages for the application of FUS for the treatment of tendon injuries. We are pursuing preclinical mouse studies for FUS and tendon healing as well. As such, this study provides an initial experimental and computational framework towards developing a novel therapy to help investigate an appropriate therapy for an ex vivo mouse model by evaluating the mechanical and thermal effects caused by the treatment. This step into investigating the mechanical loading effects is important for developing a foundation for an ex vivo setting. Therefore,

using US imaging and DIC, we hope to inform FUS dosage decisions and motivate the application of FUS as a viable treatment for tendinopathy.

1.2 Digital Image Correlation

1.2.1 Basics of DIC

DIC is a method of optically evaluating displacements and strains. It works by comparing the visual state of a material before and after a given deformation [14, 26, 32, 34, 39]. DIC is a tool used extensively in the field of biomechanics to evaluate the mechanical properties of tissues like bone, muscle, and collagenous tissues [27]. This imaging-based approach has existed for decades, but recently more efficient and elegant algorithms have greatly improved from its inception -- allowing for more accurate results in studies of mechanics and even surpassing some other methods of strain quantification as mentioned in section 1.2.2 for their application in studies of tissues [3, 11, 27].

The basic goal of DIC is to acquire displacement and strain fields within a Region of Interest (ROI) of a deforming material. First, sequential images of the material are taken from a video as it undergoes displacement and/or deformation. Then, statistical image processing algorithms and solid continuum mechanics principles are used to evaluate and interpolate the resultant strain fields [6, 14, 39].

1.2.2 Benefits and Measurement Properties

DIC has many benefits when compared to more common strain measurement tools like extensometers, strain gauges, and dial gauges [1, 14]. It has been used instead

of physical measurement tools because it performs a non-contact strain analysis with great accuracy. This is beneficial because, if done properly, it does not run the risk of altering the specimen's properties by physically affixing a measurement tool, and it is not limited by orientation such as in the case of strain gauges [21]. Furthermore, DIC can theoretically operate at any scale with a sufficient imaging resolution [6, 14]. A sufficient resolution is defined as high enough to accurately identify the scale of the displacements and strains being investigated for a particular body of work. Therefore, it is used for the methodologies in this work in the context of sensitive and small-scale experiments with a high resolution custom imaging probe on the order of 20 microns.

Another benefit is that information about the behavior of the displacement does not need to be known a priori. Generally, a strain measurement is taken using equipment that must be oriented along the anticipated straining axis and DIC is not limited by this requisite knowledge since it captures all planar strains irrespective of orientation. Instead, DIC captures all visible displacements and deformations in a user-defined ROI evaluated after the experiment is run and the images are saved [6, 39]. There are types of algorithms that can evaluate strain in real-time, but a major benefit of doing analysis in post processing with DIC is the achievement of greater accuracy [6, 14, 39]. By running the software without the constraint of active experimental sampling, the analysis can be as computationally rigorous as

the user desires based on how long they are willing to let the system run and their computational limitations [6, 14, 39].

1.2.3 DIC Requirements

DIC requires that subsequent image frames of a specimen have a sufficient quality and quantity of differentiable visual geometries. This is because each section of the images must be correlated using a statistically motivated algorithm [5, 6, 14, 26]. Often, these evaluations are done in post-processing rather than actively like in the case of some US machines which use shear-wave elastography [5, 14, 26]. The computations for DIC also necessitate a sufficiently high-resolution imaging system, and a camera is typically used [14, 31, 34].

There are different types of DIC both in 2D and 3D, but many common methods use a speckle pattern for analysis [8, 14, 31]. The speckle pattern contains many small visually contrasting shapes in sub-regions of the ROI making it easier for the algorithms to differentiate between different subsets [14, 31, 32]. Effectively, given a subset or neighborhood of pixels, the program can determine which transformed pixels in a subsequent frame most accurately match the pixel-wise structure of the previous frame. A well developed speckle pattern creates more

contrasting borders within any subset, which increases the likelihood of a successful evaluation of displacements and strains [14, 17, 31].

1.2.4 Applied vs. Natural Speckle Criterion

For a speckle based DIC analysis, the speckle pattern needs to have evenly distributed and highly contrasting visual structures, or "speckles", which are present within the specimen's ROI [7, 14, 17, 18, 31]. These speckles are typically black and white because most DIC algorithms use grayscale images for their evaluation and the contrast between black and white structures in greyscale will be

maximized [4, 7, 14, 17]. Some materials, like metals, may need a speckle pattern applied to their surfaces for DIC to work properly and effectively [4, 14].
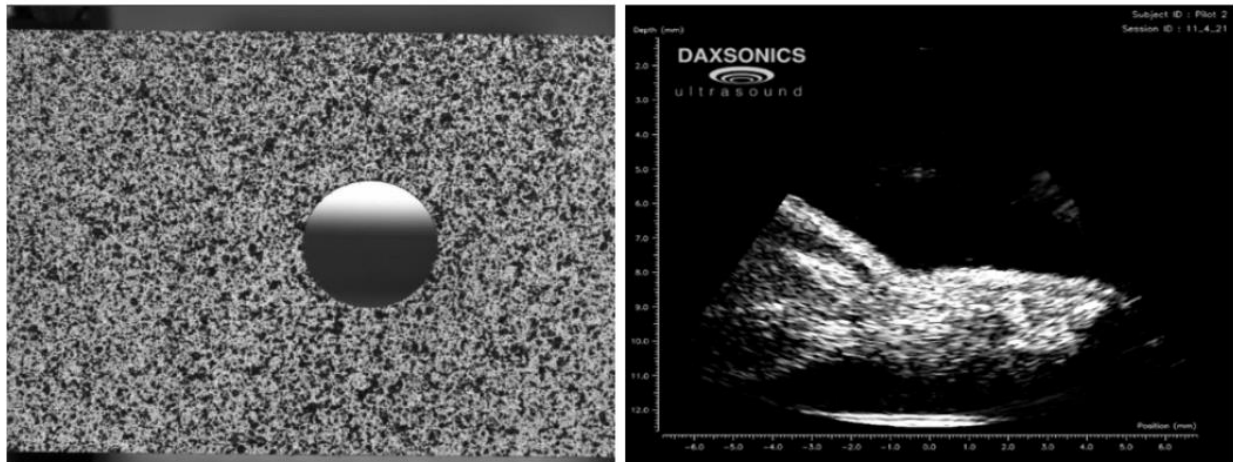

Figure 1.1: Speckle Pattern Comparison: Externally applied speckle pattern on metal specimen with circular hole (Left) [37]. US image of mouse leg tissue with a natural speckle from varying echogenicity (Right).

The current work utilizes the natural patterning of tissue that arises from US imaging for the basis of the speckle pattern as seen in Figure 1.1. US works by emitting sound waves via a transducer and detecting the echoes that reflect directly back. It achieves this using a piezoelectric material which can produce sound waves from an applied electric field in a beam pattern but can operate in reverse as well. This allows the US transducer to convert sound waves into electrical signals to be interpreted and produce a grayscale image [36]. The structures visible on the US images result from the variations in material echogenicity. Echogenicity is a measure of acoustic impedance or the resistance to the flow of energy from sound waves. The differences between tissues and materials results in the different magnitudes of energy being reflected to the transducer thereby generating the

visible structures [38]. Using these properties, we can take grayscale videos of a tissue undergoing loading, apply DIC algorithms to the extracted frames, and evaluate strain fields to investigate the resulting mechanical behavior of the tendon tissue.

This work explores the development of preliminary methodologies using two FUS therapy transducers. One methodology uses a larger 1.1 MHz therapy transducer with the imaging probe oriented orthogonally to the therapy plane. The second methodology uses a coaxial setup in which a smaller 2 MHz therapy transducer is designed with a center hole where the imaging probe can be aligned in the same orientation as the applied therapy.

Chapter 2

Experimental Methodologies - Imaging & FUS Therapies

2.1 Summary

This chapter outlines the experimental setup, applied FUS therapies, and a discussion on the procedures developed. Additionally, a detailed positioning procedure is included along with rationales for decisions made and the parameters selected for the imaging system.

A series of treatments are applied to mouse Achilles tendons with an FUS therapy transducer and treatments are recorded by means of a custom US imaging transducer and computer. Finally, the frames for DIC analysis are prepared from the saved FUS treatment video through a custom MATLAB code as referenced in Appendix B.

2.2 Calibration

2.2.1 Procedure & Materials

A calibration of the tracking technique was performed to ensure that the US imaging system was accurately displaying applied displacements. Two iterations of calibration were performed: one for the axial direction and one for the transverse direction of the US probe. The step-by-step procedure is listed in Appendix A.

To replicate the testing environment to the best of our ability, a small plastic tub filled with deionized (DI) and degassed water was placed in the center of a stereotaxic stage to match the propagation medium of the therapy transducer.

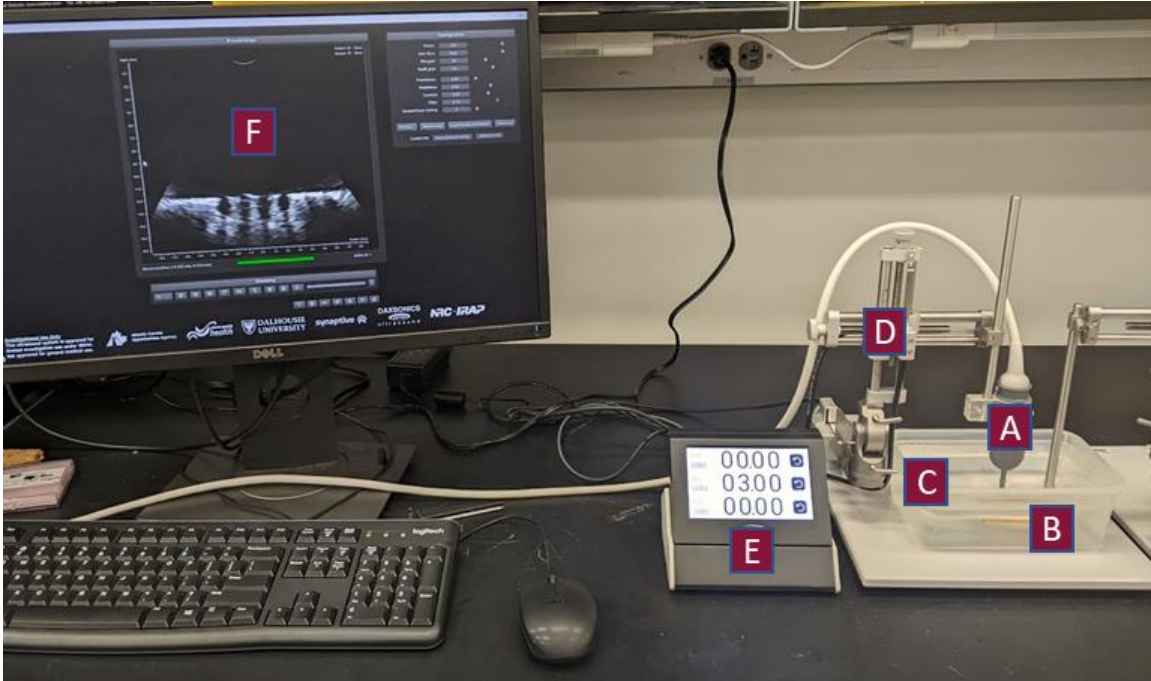Additionally, the stereotaxic devices used for the orthogonal and coaxial experimental setups were used.

Figure 2.1: Full calibration setup with imaging probe (A), PLA calibration specimen (B), water bath (C), and stereotaxic device (D) and display (E), and Sagacity imaging display (F)

A rectangular 3D printed PLA specimen, 10mm by 2mm, was fixed to a separate fixed stereotaxic arm to keep the specimen in place in the small plastic tub within view of the imaging probe. A PLA specimen was chosen because it could be easily seen with the imaging probe, it is quick, easy, and cheap to manufacture, and the design can be modified to produce identifiable regions on the PLA structure which the user can differentiate on the imaging software. It should be noted that the PLA material should not remain submerged for extended periods of time as it is possible the material may swell from taking on water through micropores in the material wall.
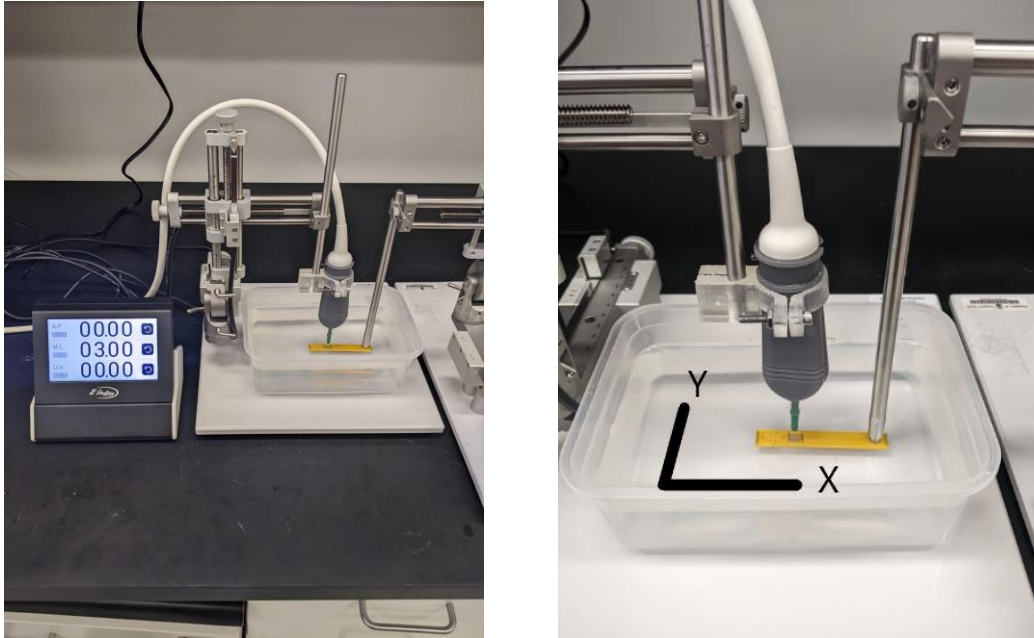
Figure 2.2: Calibration setup with electronic stereotaxic device and PLA calibration specimen with slits to view in the tracking software.

The specimen was aligned beneath the probe so that it could reliably be moved through 3 mm of displacement without leaving the field of view (FOV) of the imaging probe. This 3mm range of displacements needs to be defined for the particular axis/direction being calibrated. The initial position of the specimen was recorded through the Sagacity US imaging software. Displacement measurements were taken using the electronic readout connected to the stereotaxic instrument with an accuracy to a hundredth of a millimeter.

Measurements were taken in 0.5 mm intervals by using the stereotaxic device's controls to move the specimen. Measurements were recorded and a .png image was saved through the Sagacity imaging software for each displacement. It should be noted that it is important to save the images as a .png for analysis because this file type is "lossless" and will not be compressed.

The PLA calibration specimen was designed with a series of parallel 0.1 cm wide rectangular slits.

2.2.2 ImageJ Point Tracking

The images were loaded into ImageJ [30] - a software used for pixel-wise distance measurements, and points were chosen along the length of the specimen with identifiable structures for tracking. Points were selected manually by inspection for each frame on the basis that they could be identified qualitatively in the subsequent frames before measurement. The scale factor and resolution is determined by the number of pixels between the 0mm and 1mm tick marks on the image saved by the software. It was determined that Sagacity saves .png images with a resolution of 51 pixels/mm at an estimated magnification of 10:1 where.

Distance measurements were calculated between each successive frame based on pixel position and the resolution of the .png image. We selected 3 marked points on the specimen in its original position and displaced it through 6, 0.5 mm increments resulting in 7 total frames, 21 points, and 18 measured displacements. This was performed twice for both axial and transverse calibrations resulting in two videos for analysis in post processing.
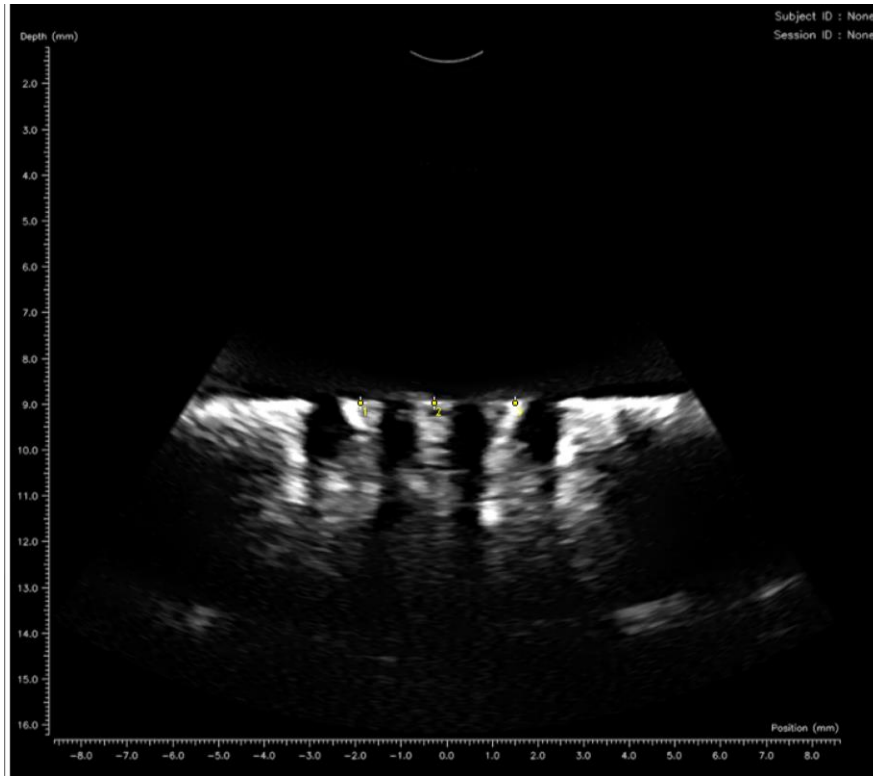
Figure 2.3: Example point tracking calibration frame in ImageJ.

2.2.3 Results

Each set of displacements between two frames was compared to the measured value of the electronic readout of 0.5 mm to yield an absolute error to a hundredth of a millimeter. A root mean square error (RMSE) was evaluated to assess the accuracy of the display compared to the stereotaxic display measurements, and a normalized RMSE (NRMSE) was calculated to compare with potential future calibration methods. An increased number of significant figures and higher resolution imaging can result in improved calibrations aiming to reduce the RMSE value. Both evaluations were done using Equations 1 and 2.

$$RMSE = \sqrt{\sum_{i=1}^{n} \frac{(y_i - \bar{y})^2}{n}} \qquad \text{(Eq. 1)}$$

$$NRMSE = \frac{RMSE}{y_{max} - y_{min}} \qquad \text{(Eq. 2)}$$

Where n is the number of displacements measured, y_i is the displacement value determined in ImageJ, y_{max} and y_{min} are the maximum and minimum displacements measured, and $\bar{y}$ is the target displacement of 1.00 mm.

Frame	Point #	Position in (mm)	
		X	Y
Reference	1	7.656863	8.745098
	2	9.27451	8.72549
	3	11.05882	8.745098
1	1	7.656863	9.245098
	2	9.235294	9.264706
	3	11.06863	9.284314
2	1	7.637255	9.781039
	2	9.310451	9.781039
	3	11.04902	9.781039
3	1	7.565353	10.29739
	2	9.271235	10.31045
	3	11.04902	10.317
4	1	7.715686	10.87255
	2	9.277784	10.83986
	3	11.04249	10.86602
5	1	7.650333	11.33661
	2	9.258176	11.34314
	3	11.05555	11.34967
6	1	7.643784	11.84641
	2	9.297392	11.86602
	3	11.09476	11.82025

Frame	Point #	Position in (mm)	
		X	Y
Reference	1	6.748373	11.85947
	2	8.375824	11.85947
	3	10.09476	11.85947
1	1	7.284314	11.84641
	2	8.931373	11.83333
	3	10.67647	11.85294
2	1	7.800647	11.85294
	2	9.375824	11.83333
	3	11.20588	11.85294
3	1	8.369275	11.84641
	2	9.977118	11.83986
	3	11.74837	11.84641
4	1	8.95751	11.8268
	2	10.54575	11.85294
	3	12.31045	11.84641
5	1	9.519608	11.85294
	2	11.12092	11.85947
	3	12.80065	11.85294
6	1	10.08171	11.83986
	2	11.63725	11.83986
	3	13.2451	11.85294

Table 2.1: X and Y position data of each point for each frame relative to the software's coordinate system converted from pixels to millimeters. (Left) Axial calibration results. (Right) Transverse calibration results.

Axial		
	X	Y
RMSE	0.050216	0.032525
NRMSE	0.225958	0.29276

Transverse		
	X	Y
RMSE	0.060189	0.012794
NRMSE	0.38375	0.244744

Table 2.2: RMSE and NRMSE values for calibration for axial (left) and transverse displacements (right).

The RMSE values for the axial X and transverse Y are errors representing the axes on which the specimen did not move, wheil the axial Y and transverse X values represent the axes on which the calibrations were performed. Given that the probe is curvilinear and the axial calibration was done relatively central on the probe, it makes sense that the X coordinate RMSE values are higher than the Y RMSE values. The RMSE values are low enough to remain accurate within the resolution of the imaging and suggests that the accuracy of the imaging system is dependent primarily on the image resolution itself. This resolution is 51 pixels/mm as mentioned previously or 0.0196 mm/pixel. This results in a reliable displacement resolution around 0.02mm since we cannot evaluate displacements with any greater accuracy on the imaging system.

This calibration procedure can be run for other US imaging systems with different resolutions as well. The NRMSE values are reported as a metric for comparison between these potential tests to be run for other work or future experiments.

2.3 Orthogonal Transducer Setup

The orthogonal setup that follows is a preliminary methodology developed awaiting the delivery of parts and construction necessary for an alternative coaxial setup described later in this document.

2.3.1 Materials

C57B1/6 male mice aged 12-16 weeks were used for the FUS therapies. The mice were obtained from other investigators at Virginia Tech, frozen at -20°C until the day of testing, and defrosted to room temperature before each experiment. Once

thawed, the hair was removed from the legs of the mice using a chemical depilatory.

The transducer equipment includes a custom FUS therapy transducer (H-101, 1.1MHz Sonic Concepts, WA, USA), a polycarbonate coupling cone (C101, Sonic Concepts, WA, USA), and a custom high frequency imaging system and probe (Sagacity Beamformer, Daxsonics Ultrasound, Inc., Halifax, Nova Scotia). Equipment and transducer specifications are listed in Appendix C.

2.3.2 Setup & Alignment Procedure

An acrylic block was fixed to the stereotaxic stage and a piece of cork was fixed to the acrylic located where the mouse leg would rest. The mice were then placed prone on the acrylic block and the leg was manipulated to orient the tendon to face the therapy transducer in the dorsal direction of the mouse. The foot was placed in full plantarflexion and the thigh and foot of the mouse were pinned at a shallow angle relative to the cork and acrylic stage as seen in Figure 2.4. This was done to fix the positioning of the tendon and avoid interference with the therapy transducer when it is descended on the tendon.
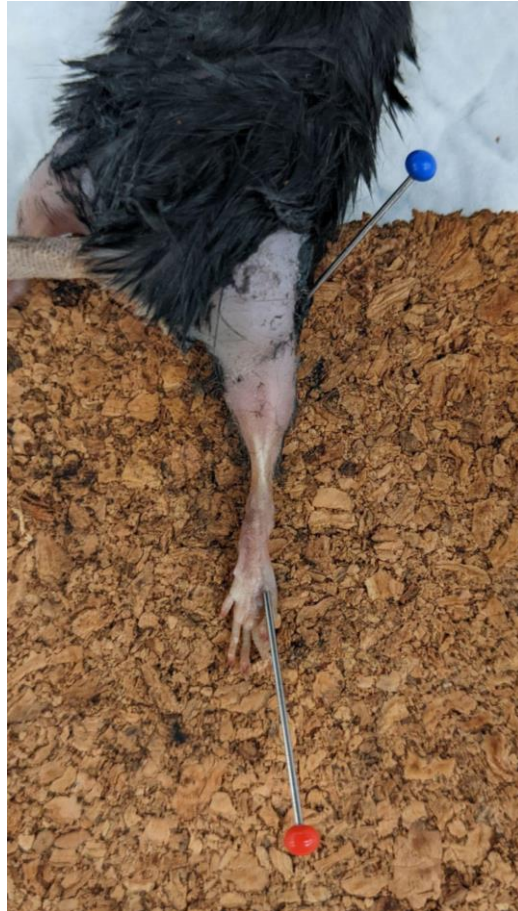
Figure 2.4: Prone mouse with leg pinned at the foot and thigh in full plantarflexion. Achilles tendon oriented dorsally.

For the orthogonal setup, the transducers are aligned such that the FUS transducer is treating the tendon in a direction perpendicular to the imaging probe's acquisition orientation as seen in Figure 2.5 below.
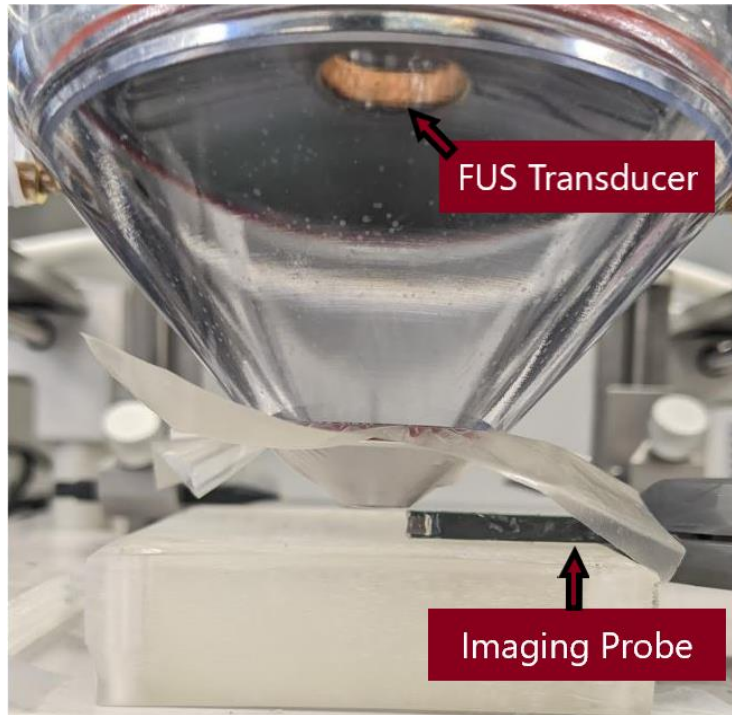
Figure 2.5: Orientation of the FUS therapy transducer and imaging probe alignment for the orthogonal setup.

The imaging computer was turned on and the software opened to view the US imaging probe's display. The imaging probe was fixed to one arm of the stereotaxic device and then oriented manually to align the imaging probe's plane with the tendon such that the tendon is viewed horizontally on the display as seen in Figure 2.6.
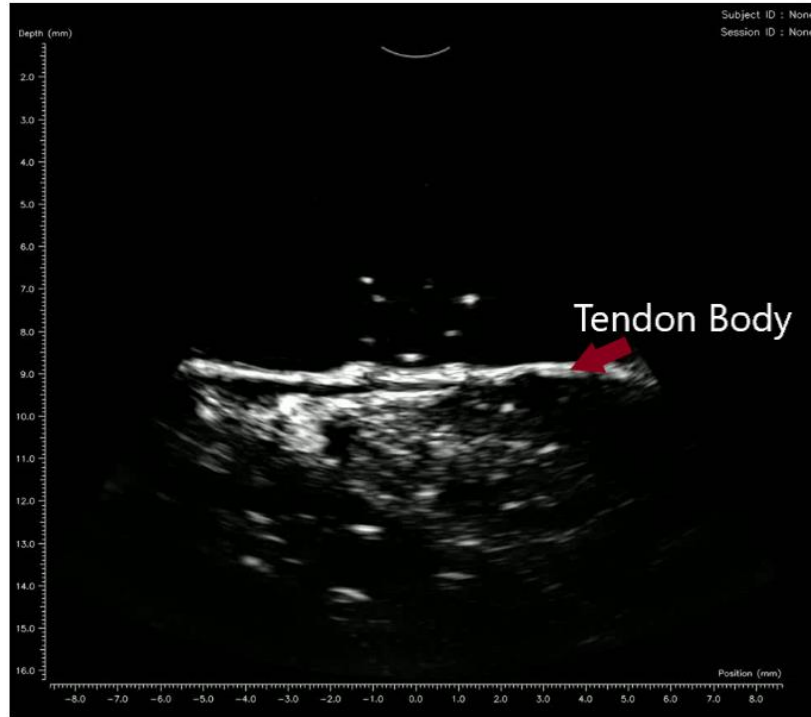
Figure 2.6: Orthogonal tendon display on Sagacity software. The tendon displays as a white strip horizontally aligned in the center of the display.

Once the imaging probe was positioned for proper viewing of the tendon, it was moved away using the stereotaxic system to align the therapy transducer's focus with the limb. A watertight coupling cone was fastened to the transducer and the cone was filled from the small opening at the bottom with DI water with a dissolved oxygen concentration <28% of saturation. The cone was filled slowly using a syringe to avoid introducing any bubbles to the propagation medium. After the cone is filled and no air bubbles are observed, an acoustically transparent membrane (Sonic Concepts, WA) was fastened to the opening, ensuring to avoid introducing air bubbles. The transducer was then affixed to the stereotaxic system and manually aligned with the mouse Achilles tendon such that the center of the opening of the cone was aligned with the middle of the tendon body.

The therapy transducer was then raised directly up, making sure that all other axes of the stereotaxic arm were fixed tightly in place. The mouse leg was liberally covered with ultrasonic gel such that the imaging transducer and tendon were both contained within. The therapy transducer was then descended onto the leg again until almost making contact with the tendon but not pressing onto it. The imaging probe was then reintroduced through the ultrasonic gel and positioned until the tendon body was visible using the display on the monitor.

A function generator (Siglent-5082, Ohio) is connected to an RF amplifier (Electronics & Innovation, 2100L) to drive the FUS transducer. The amplifier's output is connected to the transducer's corresponding matching network which subsequently connects to the FUS therapy transducer as seen in Figure 2.7.
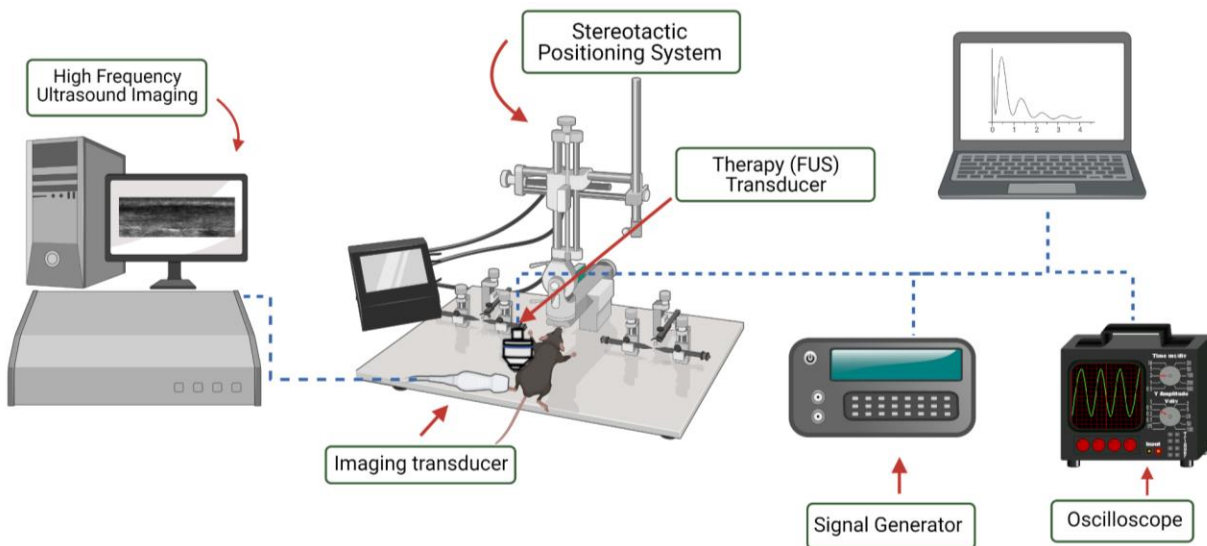

Figure 2.7: Schematic of experimental setup [23].

2.3.3 FUS Therapies

After the alignment of the transducers is completed, the electronics are connected and set to the appropriate pulsing parameters. The signal is adjusted on the function generator to the corresponding FUS therapy set. The set of therapies used for the orthogonal setup operated at 70mV peak-to-peak (pp) through a range of duty cycles from 5-100% as seen in Table 2.2. These sets were selected based on preliminary investigations into the thermal effects of varying duty cycles. The equivalent acoustic pressure was maintained for consistency at 1MPa, and the value chosen was based on the hypothesis that the mechanical effects would be sufficiently large to cause displacements viable for DIC detection and evaluation. Generally, but with potential exception, as duty cycle increases the thermal effects increase as well. Continuous sets, or 100% duty cycles, are considered primarily thermal while low duty cycles with high pressures are considered primarily mechanical for the purposes of this thesis.

Therapy Set	Driving Voltage (mVpp)	Equivalent Acoustic Pressure (MPa)	Duty Cycle
1	70	1.0	5%
2	70	1.0	10%
3	70	1.0	20%
4	70	1.0	50%
5	70	1.0	80%
6	70	1.0	100%

Table 2.2: FUS therapies 70mVpp ranging from 5-100% duty cycle

The signals are defined in this orthogonal methodology as a sine wave operating at a frequency of 1.1 MHz with an input amplitude of 70mVpp which corresponds to approximately 1MPa of acoustic pressure at the focus of the FUS therapy transducer. Duty cycles in Table 2.2 for the orthogonal setup are defined for a trigger interval of 100µs or a pulse repetition frequency (PRF) of 10kHz. Duty cycles for the coaxial setup are defined in Table 2.3 by a constant PRF of 100Hz which corresponds to a 10ms trigger interval and further defined by the number of cycles.

Duty Cycle	PRF	# of Cycles
4.6% ~ 5%	100 Hz	5
9.1% ~ 10%	100 Hz	10
18.2% ~ 20%	100 Hz	20
50.1% ~ 50%	100 Hz	55
80.1 ~ 80%	100 Hz	88
100%	100 Hz	*Continuous

Table 2.3: Number of cycles for a given duty cycle treatment at a set PRF

2.3.4 Video Acquisition & Parameters

For each experimental set the procedure is as follows: The amplifier is turned on while the channel signal on the function generator remains off. The recording is started for the imaging probe, and a timer is set simultaneously. After 5 seconds of recording, the function generator channel signal is turned on to limit delays from

the amplifier warming up. Treatment is applied for 20 seconds and the signal is turned off. The imaging software continues recording for 10 more seconds and is then terminated and saved for analysis. The tendon rests for 5 minutes and the next set of parameters is adjusted on the function generator. The procedure is then repeated for all remaining sets.

The Sagacity configuration parameters were kept constant between experiments and adjusted to achieve an imaging quality conducive to DIC analysis. The temporal averaging parameter was turned off to avoid misrepresenting time-dependent results and aliasing. The parameters used for the Sagacity software can be seen in figure 2.8 below.
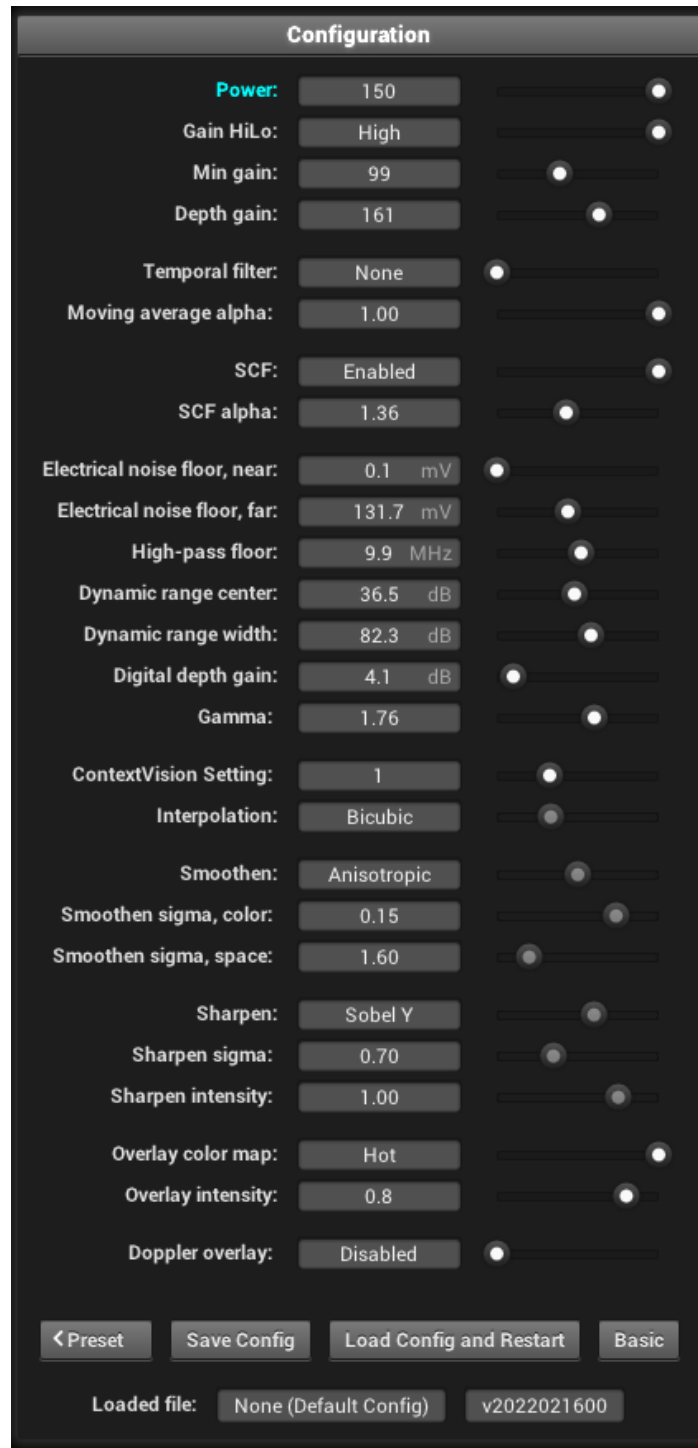
Figure 2.8: Sagacity imaging parameters for mouse Achilles tendon FUS therapy experiments.

The power should remain on maximum with Gain HiLo set to High for imaging. Min and depth gain values are set to mitigate noise on the tendon body. Moving average alpha should be set to 1 with the temporal filter turned off to eliminate any averaging. Electrical noise floors can be adjusted to clarify the image quality for slight differences between tendons as well.

2.4 Coaxial Setup

2.4.1 Materials

The same mouse model was used for the coaxial experiments as the orthogonal setup [Section 2.3.1]. The transducer equipment includes a custom 2 MHz FUS therapy transducer with a cylindrical hole to fit the same custom high frequency imaging system and probe used in the orthogonal setup (Sagacity Beamformer, Daxsonics Ultrasound, Inc., Halifax, Nova Scotia). A function generator feeding into a power supply and histotripsy pulser were used to drive the FUS transducer also designed by Daxsonics as shown in Figure 2.9.

Figure 2.9: Custom histotripsy pulser (left) power supply & amplifier (right) by Daxsonics for coaxial setup. The FUS transducer connects to OUTPUT, the function generator connects to EXT TRIG, and the power supply mediates the output to the transducer.

2.4.2 Setup and Alignment Procedure

The mouse alignment procedure is similar to the orthogonal setup with some minor differences [Section 2.3.2]. Once the mouse is placed according to the same orientation procedures, it is placed in a bath of degassed DI water. The transducers are aligned on the stereotaxic arm such that the face of the imaging probe lies flush with the aperture plane as seen in Figure 2.10.
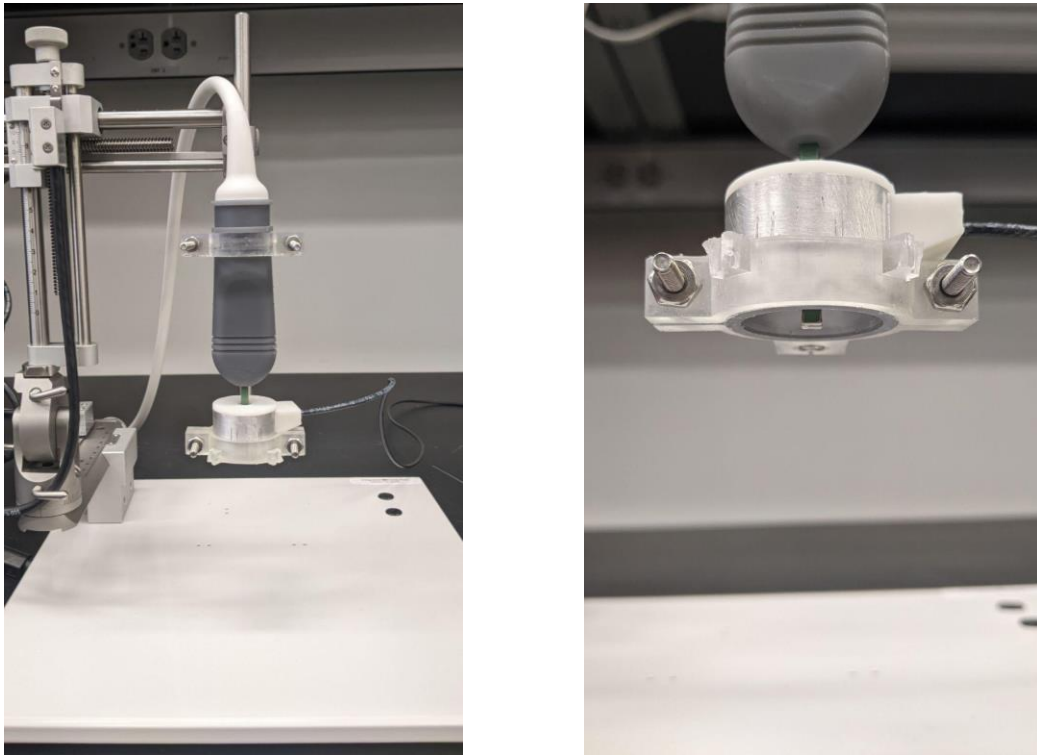

Figure 2.10: FUS and imaging transducer mounting on stereotaxic stage (left). Alignment of transducers where the imaging probe face is flush with the aperture of the FUS transducer (right).

Once the probes are fixed, they are descended on the Achilles tendon and adjusted until the display shows the desired region for treatment. The benefit of the coaxial

setup is that the imaging system can help align the focus of the FUS therapy transducer as well. The custom FUS therapy transducer made by Daxsonics has a focal length of 8mm from the aperture plane. Once the tendon body is present on the imaging monitor, the distance is adjusted so that the tendon is aligned with the 8mm depth on the screen. In this way, we can be certain that we are imaging the location of the focus and that the focus is located on the tendon body with even greater accuracy than the orthogonal setup. The entire experimental setup is illustrated in Figure 2.11.

Figure 2.11: Coaxial experimental setup (left to right): stereotaxic position electronic readout, stereotaxic stage with FUS and imaging transducers, mouse in degassed DI water bath, Daxsonics histotripsy pulser, power supply / voltage regulator, function generator.

2.4.3 FUS Therapies

Therapy Set	Driving Voltage (V)	Equivalent Acoustic Pressure (MPa)	Duty Cycle
1	3.7	1.0	5%
2	3.7	1.0	10%
3	3.7	1.0	20%
4	3.7	1.0	50%
5	3.7	1.0	80%

Table 2.4: FUS therapies for coaxial setup

Coaxial pulse sets were run at 500 cycles for every 0.5 (microseconds) and the driving voltage is different due to the design of the therapy transducer. Depending on how transducers are manufactured, different voltages equate to different equivalent acoustic pressures and must be determined by the manufacturer or through a hydrophone calibration. The value used in Table 2.4 was used based on the manufacturer's calibration.

2.4.4 Video Acquisition & Parameters

As synchronization between pulsing and imaging is not currently possible with this setup without modifications to the software and in the interest of keeping as many

variables constant between experimental setups, video acquisition was performed identically to the procedure described in section 2.3.4 for the orthogonal setup with 3 seconds of rest, 20 seconds of therapy, and 10 seconds of relaxation.

Evaluating the effects of treatment during the therapy is not possible without synchronization between the imaging and therapy transducers due to acoustic noise. This methodology would deviate in the context of synchronization as follows: Rather than evaluating the state of strain before and after therapy, the evaluation of strain will be done for the time period of active therapy in addition to the time spans pre and post treatment, and the entire time length can be evaluated in Ncorr for analysis. Once the entire time span of strain fields is evaluated, the results can be divided into sections of pre-therapy, active therapy, and post therapy. The imaging procedure does not change, but the evaluation of results will be outlined in Chapter 3.1.3.

Chapter 3

DIC & Strain Field Analysis

3.1 Ncorr - Mouse Achilles

The DIC software used for this work is an open source 2D MATLAB program called Ncorr (https://ncorr.com/index.php) [27, 39]. It has been used in applications of structural mechanics including concrete and metal material testing, mechanics of biological tissues, and high strain crack propagation for failure and fatigue tests. It is a robust user-friendly DIC program whose algorithms are designed to work for a wide variety of applications. This is beneficial because we are unsure what strains will result from various FUS therapies. Therefore this generalized toolbox is well suited to approaches which may deviate from very specific applications that other DIC algorithms may require for operation.

The guided user interface (GUI) in Ncorr allows the user to upload a series of frames, establish an ROI, edit the DIC parameters for analysis, and retain control of the computational efficiency of the program. Ncorr has also been tested against results from finite element simulations in its accuracy when compared to commercially available DIC software [5, 39].

3.1.1 Algorithm Summary

The goal of DIC is to evaluate displacements and strains of a sample undergoing some state of stress or deformation. The basis of Ncorr's algorithms is a normalized cross-correlation (Xcorr) and warping function motivated by a DIC framework called the reliability-guided DIC method (RG-DIC) developed by Pan et. al [28]. The user establishes the parameters and the program generates its

correlation criteria through a similarity metric between grayscale values at a final deformed subset as compared to a reference subset. The normalized least squares criterion, which is one of the most commonly used criteria in DIC applications, is used to generate a metric on a 0 to 1 scale to determine how likely the current or resultant transformed subset is to be correlated to the reference.

Following the correlation criteria, the Ncorr DIC algorithm runs a nonlinear optimization with the forward additive Gauss-Newton method (FA-GN) and an inverse compositional Gauss Newton method (IC-GN) completing its evaluations with a biquintic B-spline interpolation. The IC-GN method is derived from modifications to the standard application of a Gauss-Newton (GN) nonlinear iterative least squares calculation through a forward additive method creating what we typically refer to as the forward additive Gauss-Newton (FA-GN) method.

The algorithm begins from the seed point(s) selected by the user. This point is the only one that utilizes the global initial guess methods while all subsequent points are evaluated using neighboring information to establish their respective initial guesses. The order in which the algorithm makes its point-wise evaluations is illustrated in figure 3.1 taken from Ncorr's website, and a deeper dive into the

specific equations and simplifications made can be found with corresponding documentation and papers referenced [5].
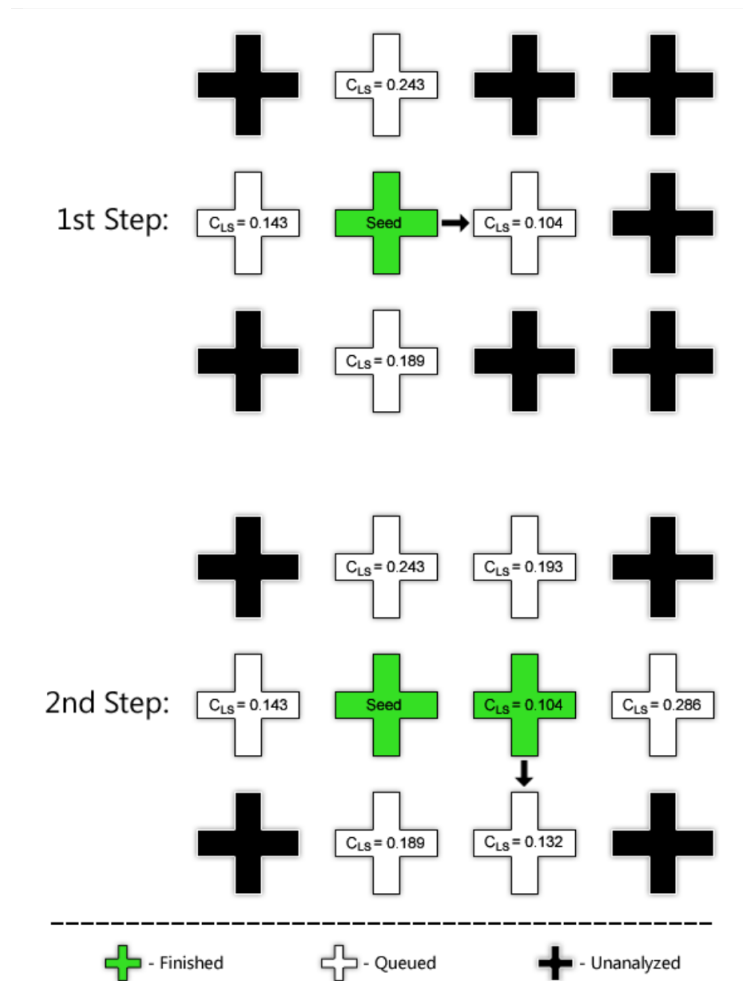

Figure 3.1: Seed propagation and displacement queue evaluation from Ncorr's website [39].

The program proceeds until all points have been queued and analyzed, at which point it terminates and is ready to evaluate the full field displacements and strains. These displacements are calculated similarly by pixel and the intermittent pixel values are interpolated to generate full fields with a biquintic B-spline. Normally, this would be a computationally demanding means of interpolation, but the decision to interpolate with such a high computational demand is motivated by the

fact that DIC analysis for this program is done in post processing. This allows for greater accuracy without dependence on quick evaluation, but does increase computation time.
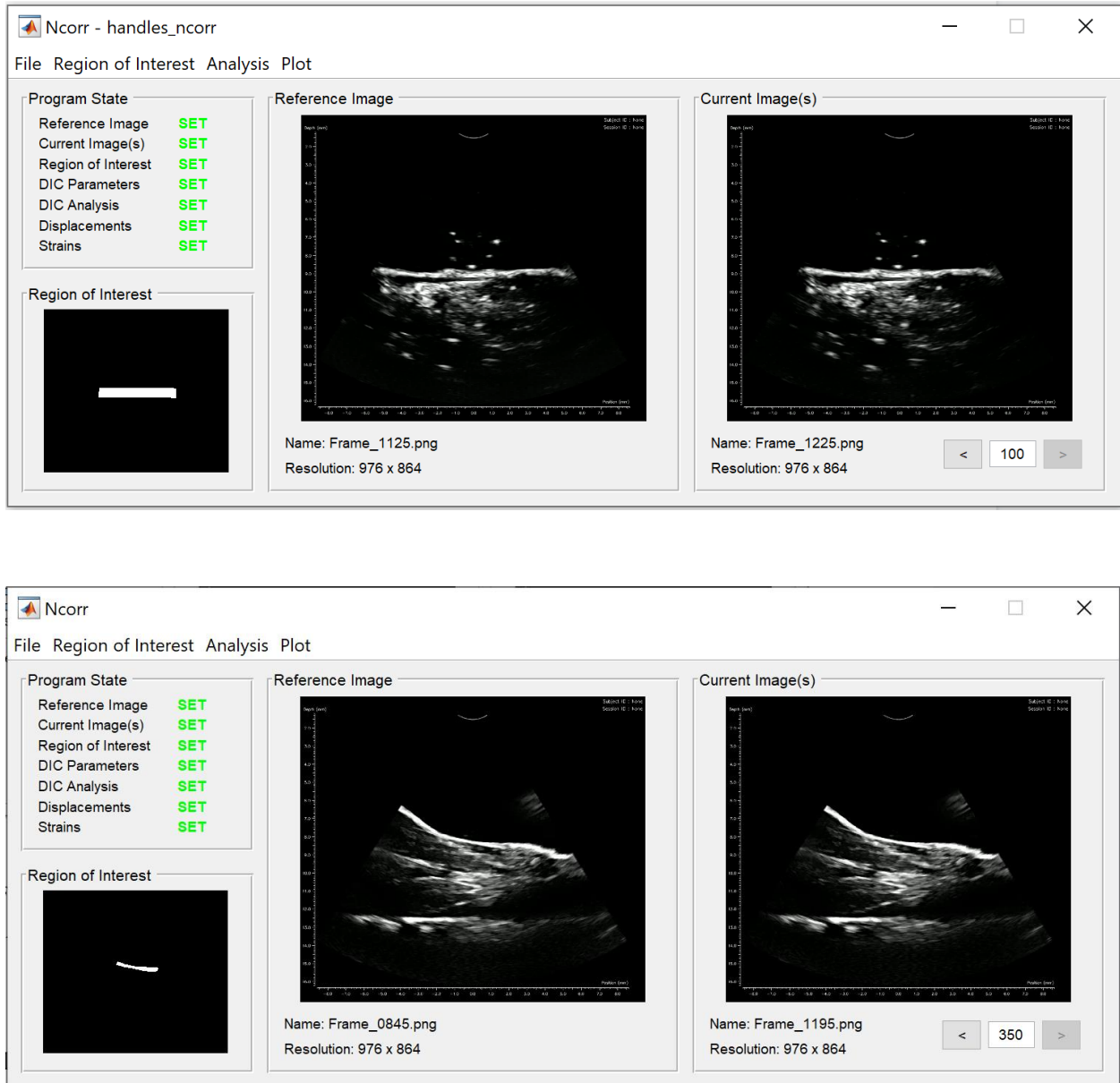
3.1.2 Frame Selection & ROI

Figure 3.2: NCorr Interface: Example of US video frames extracted from a video of a mouse Achilles tendon and leg in Ncorr's user interface. Orthogonal setup (top) and coaxial setup (bottom)

Following the recording of the experiment, the video is saved as an .mp4 with a framerate of 35 frames/s. It is then processed through a custom MATLAB script to extract .png image frames for DIC analysis referenced in Appendix B.

Once a set of frames is ready to be processed, the first step in the DIC analysis is selecting a reference image as seen in Figure 3.2. To compare the reference state of strain with the post-therapy relaxation strain, the analysis is split in two sections for one video/experiment. The first section evaluates the displacements and strains while the specimen is at rest with no externally applied treatments or loads. This acts as a noise evaluation, representing the "natural" or reference state of the tendon and leg being imaged. The second section begins immediately following the FUS therapy and lasts for 10 seconds and acts as a strain relaxation phase to help inform what kind of strains the therapy may have been imparting.

 For the reference configuration evaluation, the reference image is selected as the frame 3 seconds before the applied FUS therapy. The frames chosen for analysis include all sampled frames 3 seconds before therapy begins. This is selected by inspection following the video frame processing or by using the time at which the therapy was applied. For the duty cycles equal to or below 20%, the frames were selected based on what time the therapy was applied as recorded during experiments and a 0.2 second buffer was included to ensure no frames including the therapy were included in the reference evaluation. This was done because it cannot be optically determined when therapy begins in the video frames. For the duty cycles greater than 20% it can be optically determined when the therapy begins because the ultrasonic noise is visible.

The relaxation phase frames were determined using the same procedure but after the therapy was applied. So, 0.2 seconds after the therapy was recorded to have stopped was considered the reference frame for the second set of evaluations for one experiment. Then, 10 seconds of relaxation were selected for the relaxation phase.

The ROI is selected using the draw ROI operation in Ncorr. The ROI is drawn to include a sufficiently large portion of the tendon body and parts of the darkened area outside the border of the tendon without including tissues deeper in the leg as seen in Figure 3.3.

Figure 3.3: Example ROI for mouse Achilles tendon in Ncorr

A dark border, if available, should be included to help with the DIC analysis because dark borders help with the probability metrics used in the algorithm decisions for determining which subsets match between frames. The ROI is also selected to be as close to a rectangle as possible to retain some degree of consistency between analyses and minimize introducing sharp corners for the DIC analysis.

3.1.3 Analysis & Parameters

Once the ROI is set, the DIC parameters can be established. The parameters change based on several factors including subset radius and spacing, computation time, number of correlation iterations, seed location [14].
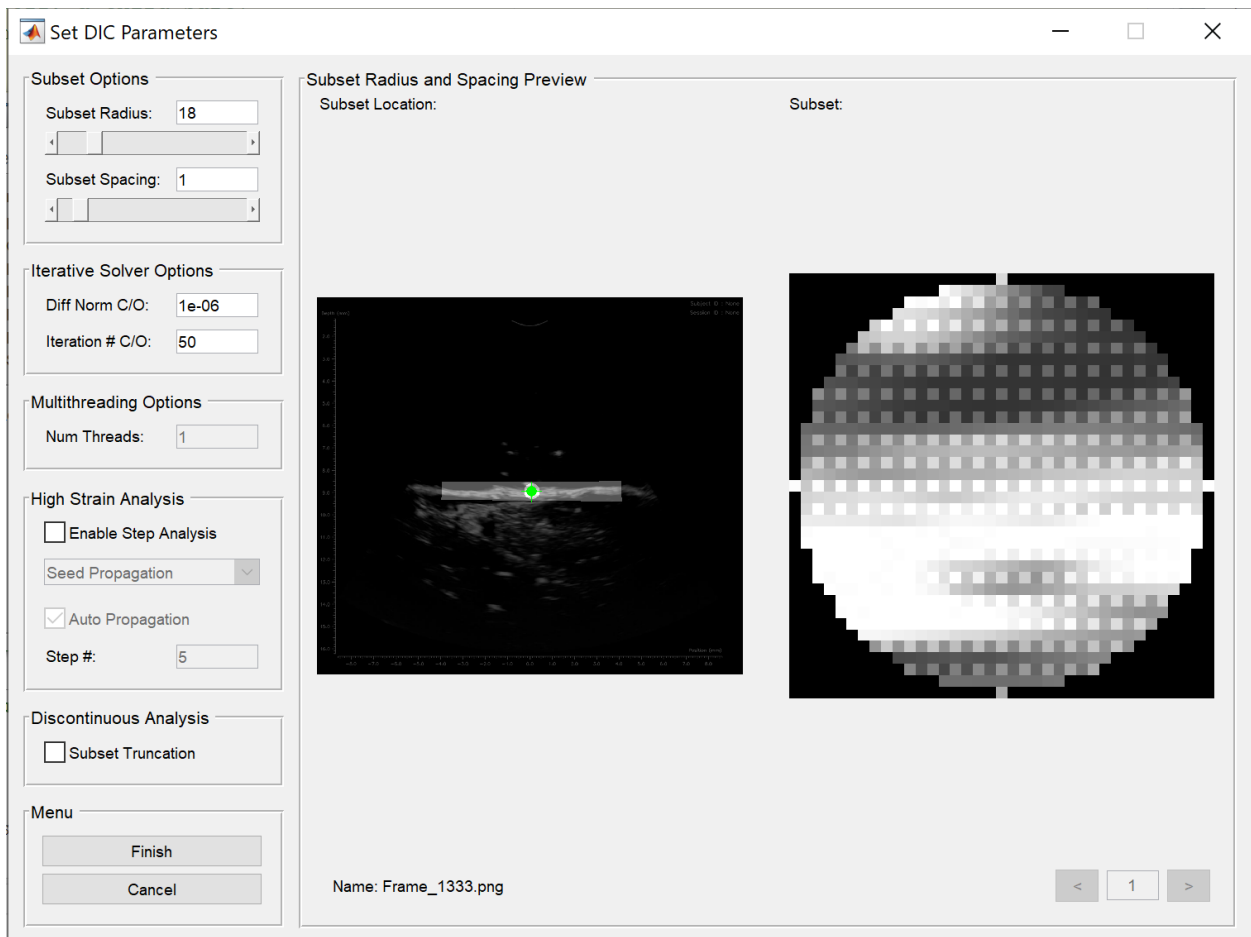
Figure 3.4: Ncorr interface for establishing subset parameters

Figure 3.4 shows the UI for setting the subset radius, subset spacing, modifications to the iterative solver, multithreading, and High Strain and Discontinuous analysis operation. The most important sections for this analysis are the Subset Options and the Iterative Solver Options. In general, the lower the subset spacing, the better the resolution results and the greater time to complete analysis. The only purpose of subset spacing in DIC is to decrease computational load, and these experiments maximized result resolution over computational time as is seen by using a subset spacing of 1. According to Ncorr's creators and corroboration by other literature on DIC, it is important to set the subset radius such that you can achieve "the smallest subset possible which does not result in noisy displacement data" [14, 27, 39]. This is typically done through trial and error, but selection criteria can be evaluated for known applications based on prior literature. Since, however, there is limited literature available for the applications of DIC in this context, it was determined through iterative evaluations that a range of values between 16-18 were sufficient to meet the iterative solver's requirements without a smoothing effect or sacrificing data. As such, a value of 18 was used across trials for consistency.

For this application we expect to see very small strains with no tearing, or failure. Therefore High Strain and Discontinuous analyses are not used. Multithreading can be used to increase computational power and reduce computation time if using a computer with multiple processors.

Seed placement must be done such that each seed evaluated for subsequent frames 'reasonably' aligns with the reference seed configuration and location. This is a relatively qualitative decision that can be informed by the number of iterations and

correlation criteria. Figure 3.5 illustrates an example of good seed correlation. It can be seen that the final seed location is a good representation of the initial reference seed with slight deformation. The number of Gauss-Newton (GN) iterations should generally be no greater than 25, or 50% of the iteration limit, if it can be helped, but it is more important that the correlation coefficient remains low. It should be noted that the GN approach usually takes more iterations than a Newton-Raphson approach, but is computationally cheaper. Therefore a much higher number of iterations is permissible. However, if the correlation coefficient goes above 0.05 it is cause for concern and close inspection or re-seeding should be done to alleviate any issues with calculations later on in the analysis.
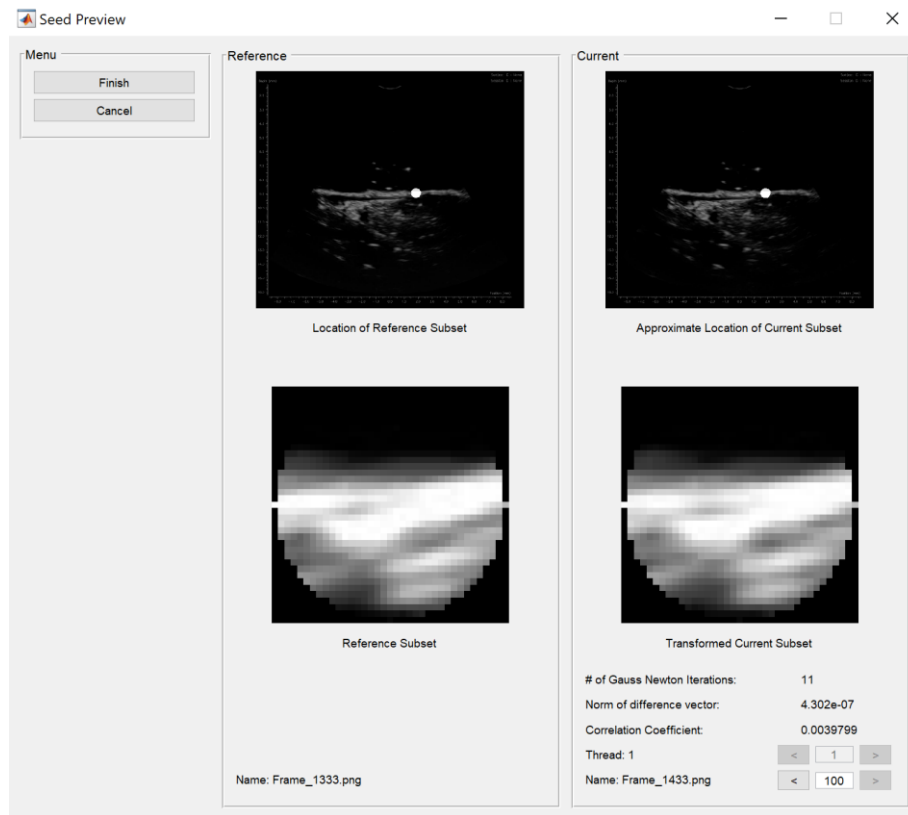

Figure 3.5: Example of good seed placement with relatively low number of Gauss-Newton Iterations

Seed placement decisions are primarily applicable to multithreading and high strain applications. Since neither were used in this application, they are not discussed in further detail.

Once the parameters and seeds are set, the DIC analysis can be performed. The final step for the user after the analysis is completed is the formatting of the displacements as seen in Figure 3.6 below.
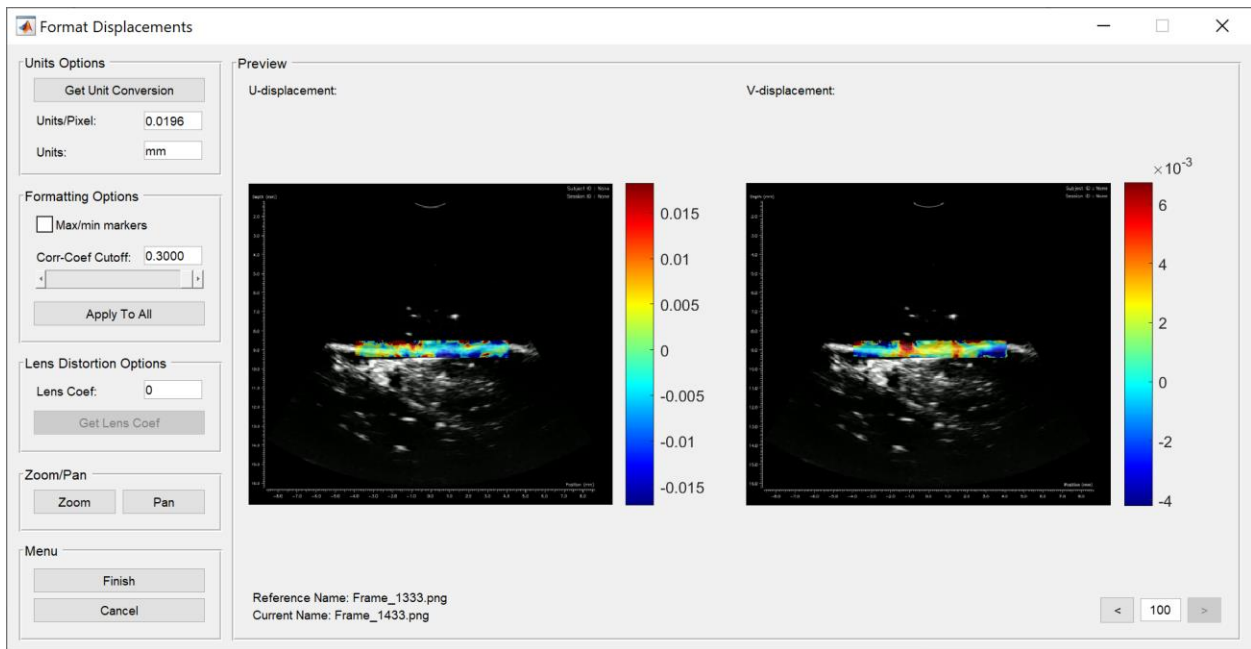

Figure 3.6: Example of formatting the displacement field in Ncorr for the reference image and all subsequent frames. X-axis or U-displacement (left) and Y-axis or V-displacement (right).

The user can set any distance unit if preferred. Based on the resolution at which Sagacity saves images, the unit conversion value was calculated to be approximately 0.0196 mm/pixel and a correlation coefficient cutoff is set to eliminate points that would be considered inaccurate by inspection. The value of 0.3 was chosen as the limit for correlation since values above 0.4 were shown to include false displacement evaluation in known static areas included in the ROI.

These parameters were equivalently applied across therapies and frames to retain a consistent metric throughout analysis. It should be noted that the lens distortion coefficient applies to optical cameras and is therefore set to 0 for this application.

After the DIC analysis is performed and the displacements are formatted, the user can take the final steps to run the Ncorr algorithms to evaluate the displacement and strain fields. Ncorr produces pint-wise fields separately for the strain components in the X-direction (Exx), Y-direction (Eyy), and shear (Exy). Plots for the Exx, Eyy, and Exy pixel-wise strain components can be generated and the bounds adjusted for scale. To evaluate the strain fields, the user must also determine the radius of subset inclusions for field evaluations. It is generally better to reduce the radius of subset evaluation to reduce the smoothing effect that results from some assumptions in Ncorr's algorithm to reduce computation time. For this application, a value below 5 for the pixel radius is sufficient to eliminate the smoothing effect substantially based on iterative testing. The strain radius is simply a computational domain defined by the user which contains the number of points for a least squares plane fit of displacement. This is done to find the plane parameters for the strain field evaluation - the specifics of which can be read in Ncorr's manual [39]. An example of the interface and suggested parameters are given in Figure 3.7 below.
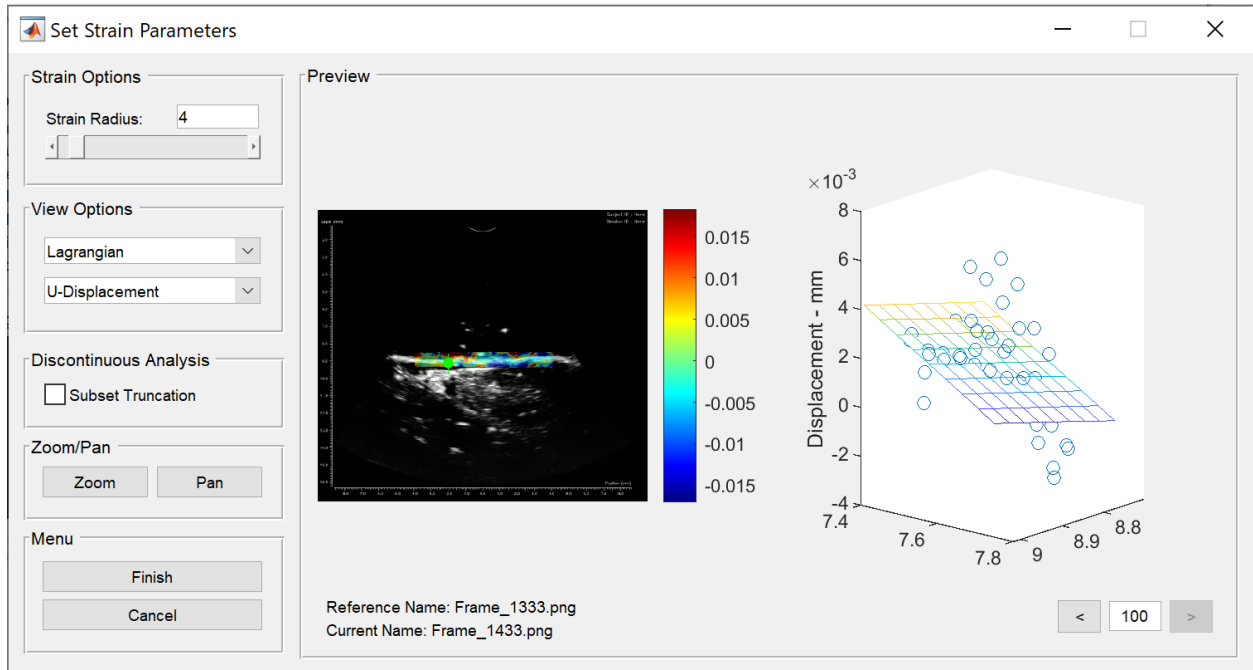
Figure 3.7: Strain parameters for Ncorr DIC analysis. Radius of subset evaluation set to 4 in a Lagrangian view without subset truncation.

3.2 Results & Discussion

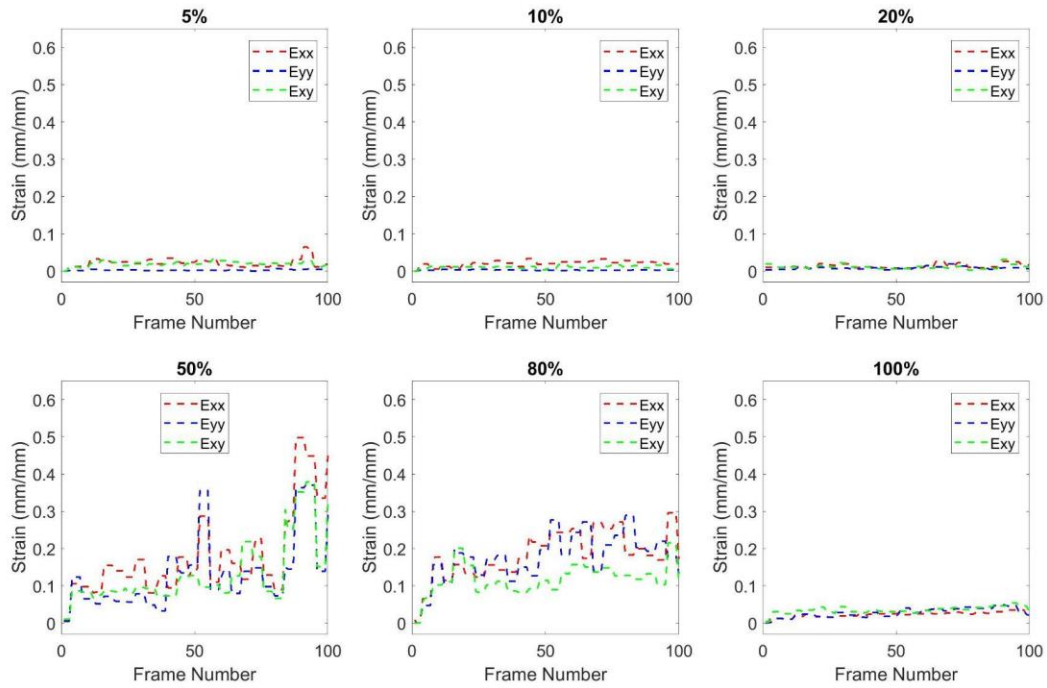## 3.2.1 Strain Field Results - Orthogonal

Figure 3.8: Maximum strain values for the Exx, Eyy, and Exy components for each frame for 70mVpp or 1 MPa at various duty cycles during 3 seconds of relaxation after treatment.
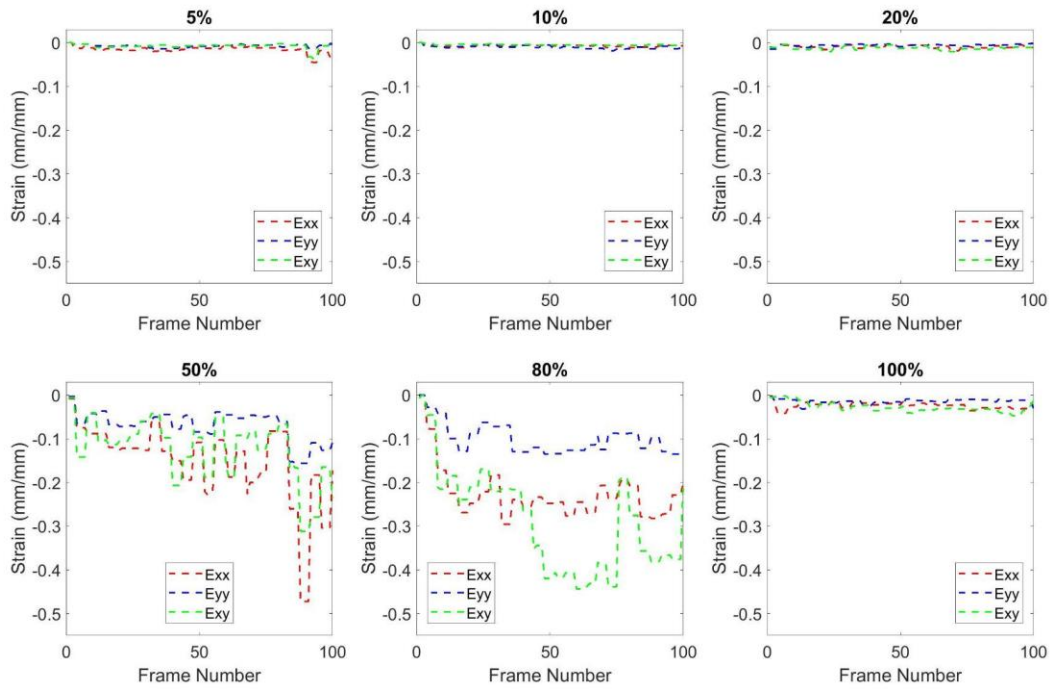
Figure 3.9: Minimum strain values for the Exx, Eyy, and Exy components for each frame for 70mVpp or 1 MPa at various duty cycles during 3 seconds of relaxation after treatment.
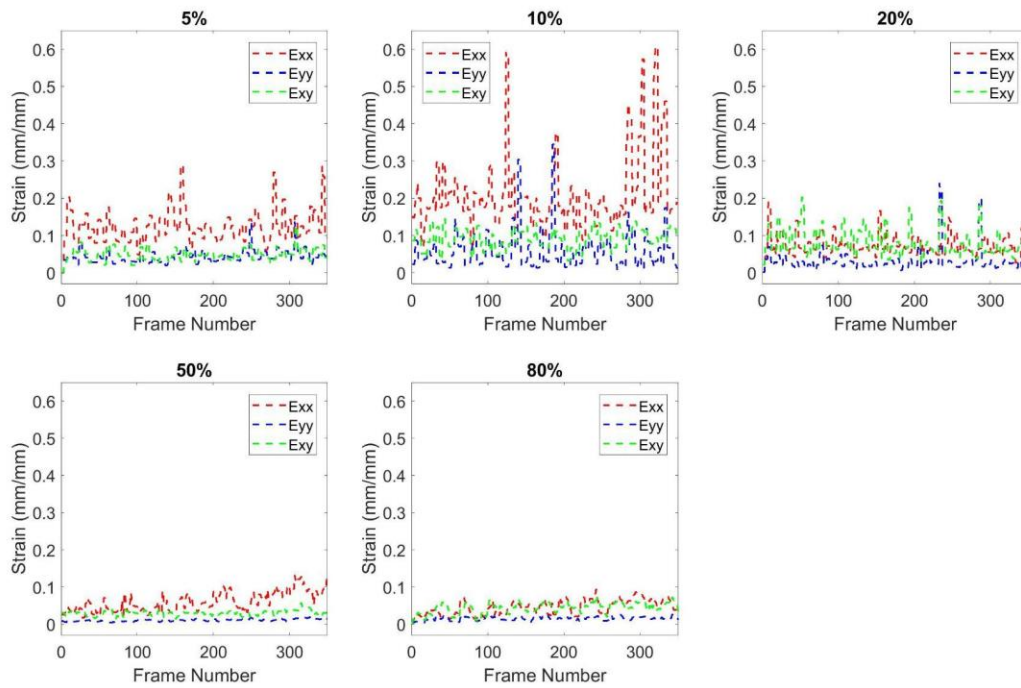
3.2.2 Strain Field Results - Coaxial

Figure 3.10: Coaxial setup maximum strain values for the Exx, Eyy, and Exy components for each frame for 1 MPa at various duty cycles during 10 seconds of relaxation after treatment.
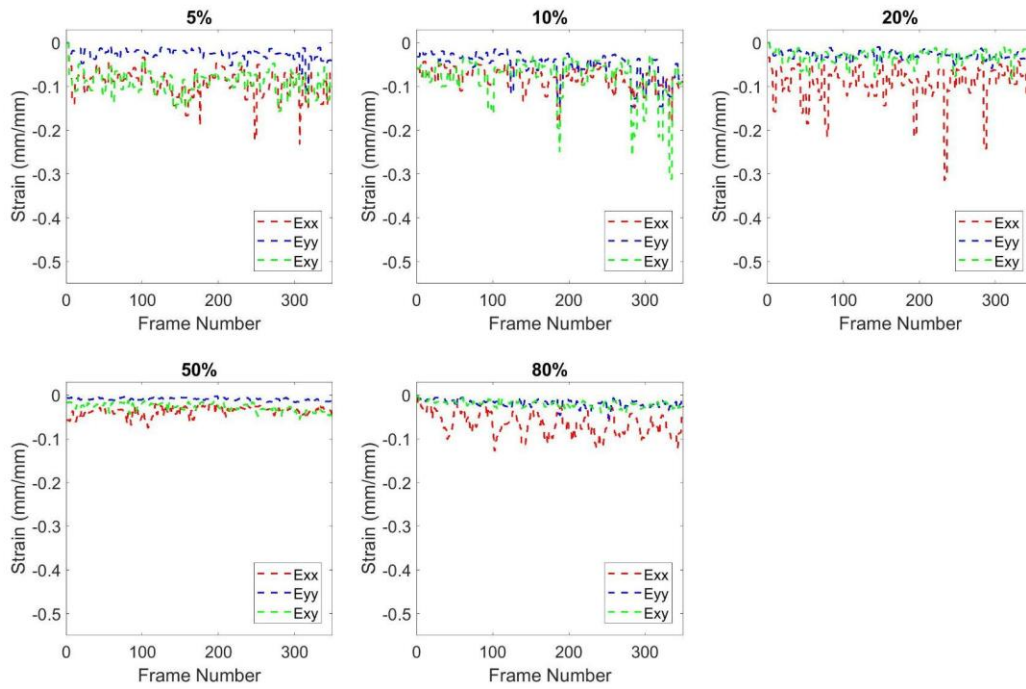
Figure 3.11: Coaxial setup minimum strain values for the Exx, Eyy, and Exy components for each frame for 1 MPa at various duty cycles during 10 seconds of relaxation after treatment.

3.2.3 Discussion

Orthogonal

Figures 3.8 and 3.9 show the maximum and minimum values for the Exx, Eyy, and Exy components of strain for a range of duty cycle percentages. It can be seen that the 50% and 80% duty cycles have a significantly higher magnitude of relaxation strain values when compared to the others. The 5%, 10%, 20%, and 100% or continuous duty cycles all show relatively low or no significant magnitude of straining effects in the relaxation phase. It is evident between the 50% and 80% duty cycle results that the Exy and Exx strain components are greater than the Eyy strain component. Interestingly, the Exx and shear components seem to be comparable. This seems to suggest that the axial straining effects are limited but the tensile effects are significant.

These results suggest that there may be a range of duty cycles for a given pressure that cause mechanical effects than others. For the orthogonal set, this range's lower bound seems to be between 20-50% duty cycle and the upper bound between 80-100% duty cycle. It is consistent with intuition that the continuous (100% duty cycle) case shows little straining effects as well because the premise of pulsed FUS is that the oscillation of applied pressures is what primarily contributes to the mechanical stresses as opposed to the thermal effects of FUS. Therefore, a continuous pulse would theoretically not produce great mechanical effects and neither would a sufficiently low duty cycle.

Coaxial

For the coaxial experimental setup, a different trend seems to emerge when compared to the orthogonal case. The lower duty cycles show greater straining effects than the higher ones. Particularly between the 10% and 20% duty cycle

48

cases shown in Figures 3.10 and 3.11 above, there is a significant magnitude of strain in the Exx direction. The coaxial case also shows some effects in the transverse direction, or Eyy component of strain, in the tendon as well. Since there are only two points in the maximum 10% case in the Eyy that show higher strain values, it is possible they are outliers, but it is too soon to tell based on these results. It should also be noted that the 80% duty cycle case seems to show an slight increase in straining effects in the Exx direction as well,

There are still many things to investigate on this front with regards to the precise boundaries of duty cycles, what kinds of duty cycles, and for what pressures these phenomena hold true. For example, a higher pressure may see a wider range of duty cycles that produce straining effects. It may also be the case that different duty cycle paradigms could produce different effects. Furthermore, the differences between a sinusoidal driving signal and a square wave or pulsed signal may have significant effects as well. It is known that square wave signals of equivalent amplitude and frequency to sinusoidal signals produce lower effective voltages, and it is common practice in the field of FUS to use pulsed waves as opposed to sine waves.

Chapter 4

Conclusion & Future Directions

4.1 Summary

This work investigated preliminary experimental and computational methodologies for quantifying and characterizing strain fields resulting from a novel FUS therapy which seeks to better understand the underlying mechanisms that contribute to healing of tendinopathic tissues. These methodologies explore the application of DIC as a tool for quantification using US imaging - an experimental means which has been validated for larger tissues undergoing mechanical loads [12, 13], but not for tissue models at this scale nor for strains resulting from FUS therapies.

The coaxial method yields greater clarity of the tendon body, more reliable alignment and view of the FUS transducer focus, and its design is more conducive for a murine model. Additionally, the coaxial setup allows for synchronicity in future experimental models which will allow for more accurate strain measurements. It was therefore determined that a coaxial setup where imaging and therapy is applied along the same axis and plane is likely a more effective methodology for acquiring strain information under FUS application.

DIC in the context of the transducers used in the coaxial setup show promise in developing more accurate quantifications of the anticipated, small strains induced by FUS as well. It is suggested by the preliminary results of the orthogonal setup that there is a range of higher duty cycles around 50-80% for a given acoustic pressure that produces greater straining effects which may be a contributing factor in tendon healing. However, the coaxial setup suggests that lower duty cycles for

the same acoustic pressure produce greater effects for a different pulsing scheme more classically used in the field of applied FUS. The changes made for the coaxial setup suggest that there is more to the pulsing schemes that requires investigation.

4.2 Limitations

4.2.1 Calibration

User identified point tracking is subject to selection bias and has an inherent limitation based on the user's discretion which may vary between users. Additionally, the physical structures of a rigid object can scatter the reflections of the US waves causing some distortion of the identifiable geometries which could reduce the accuracy. Furthermore, RMSE is a good metric for evaluating error, but the interpretation of accuracy using RMSE can be subjective. Error and the magnitude of an RMSE compared to the application is primarily motivated by the permissible tolerance of the application. In this case, the nature of the results were unknown a priori, so whether the accuracy of the imaging calibration or the resolution of the imaging system is a stronger contributing factor to the error is unknown without further validation.

4.2.2 Experimental Setup

The alignment procedures, although rigorous and carefully performed, are done manually and optically by the quantitative assessment of the researcher. Therefore, there is ample room for improvement to develop tools to place the mouse leg in a consistent orientation and align the US imaging plane with the central plane of the tendon. Further steps to create a rigid alignment between the transducers can be done to ensure the imaging probe is flush with the aperture of the coaxial FUS

transducer as well. It may also be beneficial to investigate means of fixing the limb in different stages of flexion/extension rather than just plantarflexion. Since this study was done with the leg done in full plantarflexion, it is limited by the investigation of an ex vivo tendon undergoing a particular orientation where the tendon may be crimped or compressed in some regions.

Strain fields produced in this work are preliminary assessments for the validation of DIC as a viable metric, further analysis with the coaxial methodology and therapies need to be done to confirm the characteristic strains with greater certainty.

A major limitation of the experimental setups is the inability to view the active effects of the FUS therapies. Therefore, without any synchronization between the imaging transducer and therapy transducer, a different measurement approach was taken. Additionally, the orthogonal setup images a smaller section of the tendon since it is viewed from a lateral view rather than along the full posterior facing section of the tendon being treated.

Manual alignment and qualitative parameter settings is a prominent issue throughout this preliminary work which can be improved with more sensitive and sophisticated setups that evolve from those outlined in this work.

4.2.4 DIC & Ncorr

Ncorr is a generalizable DIC toolbox which was very useful as a preliminary tool for this application. However, once the characterization of strains resulting from FUS are established with more confidence, alternative methods that are more conducive to those specific analyses can be employed to increase accuracy of

52

quantification. DIC is also limited in this application because of the alignment necessary to evaluate strains. US imaging is planar, and the nature of introducing externally applied loads whose effects are unknown may cause issues. If the tissue under investigation leaves the FOV of the imaging probe or shifts in and out of plane, then the points can no longer be correlated accurately [33]. This is mitigated to the best of our ability in this work, but any investigations into gross displacements of the leg through a range of motion will necessitate a much more sensitive alignment and restraining procedure.

4.3 Future Directions

A primary improvement in the short term of this project is a synchronization tool for the imaging transducer being developed by Daxsonics to improve the coaxial setup. The synchronization should reduce the US noise seen in the videos so that live strain analysis can be performed in the future. The water bath is a preliminary setup for a future planned design using a modified polycarbonate cone as seen in the orthogonal setup which implements the same principles for therapy. This is to make the setup generalizable between ex vivo and in vivo experiments as there will be tests done in the future on live mouse models.

Alternative methods for a more accurate calibration can include automated point tracking. Additionally, different materials and geometries can be investigated to create a more robust calibration. Material phantoms can be used as well to better evaluate the accuracy of US imaging with various tissue echogenicities. A calibration phantom developed for tendons would be ideal for this application, but no such materials have currently been developed to mimic the tissue environment of tendons for US imaging purposes.

This work is just the beginning of an exploration into using DIC with US imaging for quantifying strain fields of FUS therapies. Future work may entail determining the different effects of FUS on the distal, central, and proximal regions of the tendon. Additionally, greater resolution imaging systems and in vivo experiments will help inform the strain effects on live tissue. Improved methodologies building on these will develop more robust and accurate results and inform decisions on FUS therapies.

References

[1] adm_stress, "Digital Image Correlation to Measure Strain and Displacement," *Stress Engineering Services, Inc*, Sep. 14, 2020. https://www.stress.com/dic-to-measure-large-areas-of-strain-displacement/ (accessed Jul. 04, 2022).

[2] B. M. Andres and G. A. C. Murrell, "Treatment of Tendinopathy: What Works, What Does Not, and What is on the Horizon," *Clin Orthop Relat Res*, vol. 466, no. 7, pp. 1539–1554, Jul. 2008, doi: 10.1007/s11999-008-0260-1.

[3] P. E. Anuta, "Spatial Registration of Multispectral and Multitemporal Digital Imagery Using Fast Fourier Transform Techniques," *IEEE Transactions on Geoscience Electronics*, vol. 8, no. 4, pp. 353–368, Oct. 1970, doi: 10.1109/TGE.1970.271435.

[4] Y. Barranger, P. Doumalin, J. C. Dupré, and A. Germaneau, "Strain Measurement by Digital Image Correlation: Influence of Two Types of Speckle Patterns Made from Rigid or Deformable Marks: **Strain Measurement by Digital Image Correlation**," *Strain*, vol. 48, no. 5, pp. 357–365, Oct. 2012, doi: 10.1111/j.1475-1305.2011.00831.x.

[5] J. Blaber, B. Adair, and A. Antoniou, "Ncorr: Open-Source 2D Digital Image Correlation Matlab Software," *Exp Mech*, vol. 55, no. 6, pp. 1105–1122, Jul. 2015, doi: 10.1007/s11340-015-0009-1.

[6] L. Cristofolini, "Overview of Digital Image Correlation," 2015, pp. 187–213. doi: 10.1007/978-3-319-06086-6_5.

[7] F. Dandois *et al.*, "Validated Ultrasound Speckle Tracking Method for Measuring Strains of Knee Collateral Ligaments In-Situ during Varus/Valgus

Loading," *Sensors (Basel)*, vol. 21, no. 5, p. 1895, Mar. 2021, doi: 10.3390/s21051895.

[8] Y. L. Dong and B. Pan, "A Review of Speckle Pattern Fabrication and Assessment for Digital Image Correlation," *Exp Mech*, vol. 57, no. 8, pp. 1161–1181, Oct. 2017, doi: 10.1007/s11340-017-0283-1.

[9] F. Feng, A. Mal, M. Kabo, J. Wang, and Y. Bar-Cohen, "The mechanical and thermal effects of focused ultrasound in a model biological material," *The Journal of the Acoustical Society of America*, vol. 117, pp. 2347–55, May 2005, doi: 10.1121/1.1873372.

[10] B. Girgis and J. A. Duarte, "Physical therapy for tendinopathy: An umbrella review of systematic reviews and meta-analyses," *Phys Ther Sport*, vol. 46, pp. 30–46, Nov. 2020, doi: 10.1016/j.ptsp.2020.08.002.

[11] S. Hensley, M. Christensen, S. Small, D. Archer, E. Lakes, and R. Rogge, "Digital image correlation techniques for strain measurement in a variety of biomechanical test models," *Acta Bioeng Biomech*, vol. 19, no. 3, pp. 187–195, 2017.

[12] R. J. Hodgson, P. J. O'Connor, and A. J. Grainger, "Tendon and ligament imaging," *Br J Radiol*, vol. 85, no. 1016, pp. 1157–1172, Aug. 2012, doi: 10.1259/bjr/34786470.

[13] K. Holak, P. Kohut, A. Młyniec, M. Ekiert, K. Tomaszewski, and T. Uhl, "THE USE OF DIGITAL IMAGE CORRELATION IN THE STUDY OF ACHILLES TENDON STRAIN FIELD," *Mechanics and Control*, vol. 34, no. 1, Art. no. 1, 2015, doi: 10.7494/mech.2015.34.1.19.

[14] International Digital Image Correlation Society *et al.*, "A Good Practices Guide for Digital Image Correlation," International Digital Image Correlation Society, Oct. 2018. doi: 10.32720/idics/gpg.ed1.

[15] P. T. Karjalainen *et al.*, "MR imaging of overuse injuries of the Achilles tendon," *AJR Am J Roentgenol*, vol. 175, no. 1, pp. 251–260, Jul. 2000, doi: 10.2214/ajr.175.1.1750251.

[16] J. Kubanek, "Neuromodulation with transcranial focused ultrasound," *Neurosurg Focus*, vol. 44, no. 2, p. E14, Feb. 2018, doi: 10.3171/2017.11.FOCUS17621.

[17] W. S. LePage, J. A. Shaw, and S. H. Daly, "Optimum Paint Sequence for Speckle Patterns in Digital Image Correlation," *Exp Tech*, vol. 41, no. 5, pp. 557–563, Oct. 2017, doi: 10.1007/s40799-017-0192-3.

[18] G. Lionello, C. Sirieix, and M. Baleani, "An effective procedure to create a speckle pattern on biological soft tissue for digital image correlation measurements," *Journal of the Mechanical Behavior of Biomedical Materials*, vol. 39, pp. 1–8, Nov. 2014, doi: 10.1016/j.jmbbm.2014.07.007.

[19] C. Loiacono *et al.*, "Tendinopathy: Pathophysiology, Therapeutic Options, and Role of Nutraceutics. A Narrative Literature Review," *Medicina (Kaunas)*, vol. 55, no. 8, p. 447, Aug. 2019, doi: 10.3390/medicina55080447.

[20] T. Luyckx, M. Verstraete, K. De Roo, W. De Waele, J. Bellemans, and J. Victor, "Digital image correlation as a tool for three-dimensional strain analysis in human tendon tissue," *J Exp Orthop*, vol. 1, no. 1, p. 7, Dec. 2014, doi: 10.1186/s40634-014-0007-8.

[21] S. Mak, "Introduction to Strain Gages", Accessed: Jul. 04, 2022. [Online]. Available: https://www.academia.edu/4776559/Introduction_to_Strain_Gages

[22] W. Matthews, R. Ellis, J. Furness, and W. A. Hing, "The clinical diagnosis of Achilles tendinopathy: a scoping review," *PeerJ*, vol. 9, p. e12166, Sep. 2021, doi: 10.7717/peerj.12166.

[23] C. Meduri, E. Vlaisavljevich, P. G. Brolinson, and V. M. Wang, "Ultrasound Stimulation of Tendon Healing: Current Strategies and Opportunities for Novel Therapeutic Approaches," in *Regenerative Rehabilitation: From Basic Science to the Clinic*, S. M. Greising and J. A. Call, Eds. Cham: Springer International Publishing, 2022, pp. 331–358. doi: 10.1007/978-3-030-95884-8_10.

[24] Y. Meng, K. Hynynen, and N. Lipsman, "Applications of focused ultrasound in the brain: from thermoablation to drug delivery," *Nat Rev Neurol*, vol. 17, no. 1, pp. 7–22, Jan. 2021, doi: 10.1038/s41582-020-00418-z.

[25] A. Neviaser, N. Andarawis-Puri, and E. Flatow, "Basic mechanisms of tendon fatigue damage," *J Shoulder Elbow Surg*, vol. 21, no. 2, pp. 158–163, Feb. 2012, doi: 10.1016/j.jse.2011.11.014.

[26] G. Okotie, S. Duenwald-Kuehl, H. Kobayashi, M.-J. Wu, and R. Vanderby, "Tendon Strain Measurements With Dynamic Ultrasound Images: Evaluation of Digital Image Correlation," *Journal of Biomechanical Engineering*, vol. 134, no. 2, p. 024504, 2012.

[27] M. Palanca, G. Tozzi, and L. Cristofolini, "The use of digital image correlation in the biomechanical area: A review," *International Biomechanics*, vol. 3, pp. 1–21, Dec. 2015, doi: 10.1080/23335432.2015.1117395.

[28] B. Pan, K. Li, and W. Tong, "Fast, Robust and Accurate Digital Image Correlation Calculation Without Redundant Computations," *Exp Mech*, vol. 53, no. 7, pp. 1277–1289, Sep. 2013, doi: 10.1007/s11340-013-9717-6.

[29] E. Peck, E. Jelsing, and K. Onishi, "Advanced Ultrasound-Guided Interventions for Tendinopathy," *Phys Med Rehabil Clin N Am*, vol. 27, no. 3, pp. 733–748, Aug. 2016, doi: 10.1016/j.pmr.2016.04.008.

[30] C. A. Schneider, W. S. Rasband, and K. W. Eliceiri, "NIH Image to ImageJ: 25 years of image analysis," *Nat Methods*, vol. 9, no. 7, Art. no. 7, Jul. 2012, doi: 10.1038/nmeth.2089.

[31] H. Schreier, J.-J. Orteu, and M. A. Sutton, *Image Correlation for Shape, Motion and Deformation Measurements*. Boston, MA: Springer US, 2009. doi: 10.1007/978-0-387-78747-3.

[32] L. C. Slane and D. G. Thelen, "The Use of 2D Ultrasound Elastography for Measuring Tendon Motion and Strain," *J Biomech*, vol. 47, no. 3, pp. 750–754, Feb. 2014, doi: 10.1016/j.jbiomech.2013.11.023.

[33] M. A. Sutton, J. H. Yan, V. Tiwari, H. W. Schreier, and J. J. Orteu, "The effect of out-of-plane motion on 2D and 3D digital image correlation measurements," *Optics and Lasers in Engineering*, vol. 46, no. 10, pp. 746–757, Oct. 2008, doi: 10.1016/j.optlaseng.2008.05.005.

[34] D. Turner, P. Crozier, and P. Reu, "Digital Image Correlation Engine v.3.0," Sandia National Laboratories (SNL), Albuquerque, NM, and Livermore, CA (United States), DICE, Oct. 2015. doi: 10.11578/dc.20171025.1658.

[35] S. J. Warden, Z. S. Kiss, F. A. Malara, A. B. T. Ooi, J. L. Cook, and K. M. Crossley, "Comparative accuracy of magnetic resonance imaging and ultrasonography in confirming clinically diagnosed patellar tendinopathy," *Am J Sports Med*, vol. 35, no. 3, pp. 427–436, Mar. 2007, doi: 10.1177/0363546506294858.

[36] J. Wong, "How Do Ultrasonic Transducers Work," *Beijing Ultrasonic*, Apr. 08, 2013. https://www.bjultrasonic.com/how-ultrasonic-transducers-work/ (accessed Jul. 04, 2022).

[37] "Digital Image Correlation – PhotoDyn." https://photodyn.org/tools/dic-method (accessed May 29, 2022).

[38] "Mechanisms of Action," *Focused Ultrasound Foundation*. https://www.fusfoundation.org/the-technology/mechanisms-of-action/ (accessed Jul. 04, 2022).

[39] "Ncorr - Open source 2D digital image correlation MATLAB software." https://ncorr.com/index.php (accessed May 29, 2022).

Appendices

Appendix A: Calibration Procedure

1. Set up imaging probe and calibration specimen in water for a reference position
   a. Keep the US display on to verify the positioning.
   b. Determine a position such that you can get as many 0.5mm measurements as necessary (6 intervals in this case). The specimen should start at a reference point such that when it is displaced, the rest of your measurements can be taken within the view of the ultrasound imaging probe.
2. Record the reference position on the stereotaxic device or zero out the display
3. Take a reference image screenshot on the Sagacity software
   a. Ensure the images are saved to the folder and rename the reference image appropriately at this time.
4. Use the stereotaxic system to displace the specimen by 0.5mm using the electronic display to an accuracy of 0.01mm.
5. Take a screenshot of the displaced specimen
   a. Rename the new file after each screenshot is taken to avoid mislabelling in post
   b. NOTE: moving the probe away from the specimen may show a displacement on the screen in the opposite direction depending on the probe alignment.
6. Repeat steps 4-6 until all displacement frames have been taken.

Appendix B: MATLAB Image-Processing

clc; clear; clf; close all; imtool close all;

%% VIDEO PROCESSING

% Last Edited: 6/15/2022 By: Steven Salazar

% Purpose: This script is designed to take in a video file and extract the

% frames from that file as .png images. Below there are some things you should know and do before

% running this script - primarily what it will ask of you to run properly.s

%% [I] Troubleshooting

% "Change the Directories if running script from a different computer"

% Anytime you are running this script, it should be able to handle itself

% without much adjustment to directory, but every so often MATLAB has a fit and

% you need to manually add paths. You will also need to include the NCorr

pathway for your

% computer if it is not contained in the operating directory of this script.

% Naming Frame Folders

% You must follow the NCorr rules for file naming as outlined in the

% Appendix section at the end of this script.

%% Add Directory Locations

%EDIT THE NEXT LINE FOR THE CORRECT DIRECTORY FOLDER

% Add path for location of NCorr

addpath('C:\Users\steve\Desktop\Masters_Project\ncorr_2D_matlab-master');

```matlab
strMessage = sprintf('Select the Directory to save Frame Folders');

response1 = questdlg(strMessage, 'File Selection', 'Select a Folder', 'Cancel', 'Select

a Folder');

if strcmpi(response1, 'Select a Folder')

    file_directory = uigetdir;

    addpath(file_directory);

else

    return;

end


%% Frames to be Extracted - File Name

prompt = {'Name a New Folder for the Frames to be Extracted.'};

dlgtitle = 'Saved Frames Folder Name';

dims = [1 120];

definput = {'FrameFolderNameHere'};

FramesFolderName = inputdlg(prompt,dlgtitle,dims,definput);


%% Generate the Frame Folder

%Generates folder for the new Frames to be made in the Frame_Files directory.

if isempty(dir(strcat(file_directory,'\',FramesFolderName{:}))) == 1

    mkdir(file_directory, FramesFolderName{:});

end

outputFolder = dir(strcat(file_directory,'\',FramesFolderName{:})).folder;


%% Video File

mov_name = {};
```

```matlab
% Get Video File
if ~exist(mov_name, 'file')
        strErrorMessage = sprintf('Select a Video file for Processing');
        response = questdlg(strErrorMessage, 'File Selection', 'Select a Video File',
'Cancel', 'Select a Video File');
        if strcmpi(response, 'Select a Video File')
                [baseFileNameNoExt, folderName, FilterIndex] = uigetfile('*.mp4');
                if ~isequal(baseFileNameNoExt, 0)
                        mov_name = fullfile(folderName, baseFileNameNoExt);
                else
                        return;
                end
        else
                return;
    end
end

if ~isempty(mov_name) == 1
    strErrorMessage = sprintf('You have selected the following file:\n%s\nYou can
continue, Choose a new file, or cancel', mov_name);
    response = questdlg(strErrorMessage, 'Verify Selected File', 'Continue', 'Choose
a new file', 'Cancel', 'Continue');
    if strcmpi(response, 'Choose a new file')
        [baseFileNameNoExt, folderName, FilterIndex] = uigetfile('*.mp4');
        if ~isequal(baseFileNameNoExt, 0)
            mov_name = fullfile(folderName, baseFileNameNoExt);
        else
```

```matlab
            return;
        end
    elseif strcmpi(response, 'Cancel')
        return;
    end
end


%% Convert Video File to Frames in Folder
mov = VideoReader(mov_name); % Reads the video file and imports video data.
numberOfFrames = mov.NumFrames;    % Determine how many frames there are
in imported video (mov).

tic;
for frame = 1 : numberOfFrames
    % Extract the frame from the movie structure.
    thisFrame = read(mov, frame);
    % Create a filename. Can Change Name based on Trial if desired
    % (FOLLOW NCORR RULES FOR FILE WRITING!!!)
    outputBaseFileName = sprintf('Frame_%4.4d.png', frame); %updates frame
number on file
    outputFullFileName = fullfile(outputFolder, outputBaseFileName);
    % Write image file to selected file with updated frame number.
    imwrite(thisFrame, outputFullFileName, 'png');
end
frame_process_time = toc
```

Appendix C: Equipment Specifications

Equipment is specified if it is used in the setup for (orthogonal, coaxial, or both).

Oscilloscope (Both)

Tektronix; TBS 2000B Series Digital Oscilloscope

{TBS2202B // 200 MHz // 2GS/s}

1MΩ // 13pF ≤ 300V RMS CAT II

Function Generator (Both):

Tektronix; AFG31000 Series Arbitrary Function Generator

{AFG31102 //100MHz // 1GS/s}

RF Amplifier (Orthogonal):

E&I; 2100L RF Amplifier

Frequency Range: 10 kHz - 12 MHz

Power: 100 Watts

Sonic Concepts H-101 ∅64mm FUS Transducer (Orthogonal):

https://sonicconcepts.com/wp-content/uploads/2017/07/H-%C3%9864-Rev.-B.pdf

Daxsonics FUS Transducer w/ hole (Coaxial):

Frequency: 2MHz

Focal length: 8mm {distance from aperture plane}

Diameter (Outer): 30.2mm

Diameter (Inner): 6.5mm

Height: 23.0mm